THE JOURNAL OF PHYSICAL CHEMISTRY C

Feature Article

Cite This: J. Phys. Chem. C 2019, 123, 8469−8483

pubs.acs.org/JPCC

Plasmon-Driven Reaction Mechanisms: Hot Electron Transfer versus Plasmon-Pumped Adsorbate Excitation

Tefera E. Tesema, Bijesh Kafle, and Terefe G. Habteyes*

Department of Chemistry and Chemical Biology and Center for High Technology Materials, University of New Mexico, Albuquerque, New Mexico 87131, United States

ABSTRACT: Photochemistry that can be driven at low incident photon flux on optically excited plasmonic nanoparticles is attracting increasing research interest because of the fundamental need to combine surface reaction and in situ spectroscopy as well as the opportunity that plasmon-driven reactions may offer a pathway for efficient conversion of solar energy into fuel. In mechanistic studies of plasmon-driven reactions to date, a great deal of emphasis is given to hot electron transfer. The results summarized in this Feature Article indicate that photochemistry on plasmonic nanoparticles can be induced by hot electron transfer from the nanoparticle to an unoccupied orbital of the adsorbate and/or by plasmon-pumped electron transition from an occupied molecular orbital to an unoccupied molecular orbital of the adsorbate. The branching photochemical reaction of *para*-aminothiophenol on the plasmonic gold surface depending on the presence of a cetyltrimethylammonium bromide surface ligand that influences the hot electron concentration is used to highlight reactions driven by hot carriers. The importance of plasmon-pumped electronic excitation of adsorbates in initiating surface photochemistry is demonstrated based on the N-demethylation of methylene blue (MB) on gold nanostructures depending on excitation wavelengths. At excitation wavelength that overlaps with the resonances of MB and the gold nanoparticles, conversion of MB to thionine is observed in the presence of oxygen in the atmosphere and water in the surface−molecule complex. Considering that MB is a well-known photosensitizer, this observation suggests that the photochemical N-demethylation reaction involves singlet oxygen that can be generated via energy transfer from the MB triplet excited state to the O_2 triplet ground state.

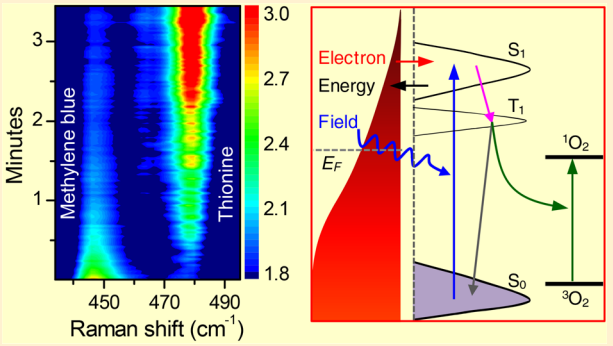

1. INTRODUCTION

Optical excitation of localized surface plasmon resonances (collective oscillation of conduction electrons) of metal (gold, silver, copper, etc.) nanoparticles creates an enhanced surface field confined to nanoscale volume that is defined by the size of the nanoparticles as well as by the gaps between the nanoparticles.[1−4] The magnitude of the local field can be several orders larger than that of the incident excitation field.[5−7] As a result, for molecules adsorbed on the surface of the plasmonic nanoparticles, their spectroscopic signal can be enhanced enormously by the plasmon near field, an evanescent wave that decays exponentially with distance from the surface. The near-field effect has led to the development of highly sensitive spectroscopy, notably surface-enhanced Raman scattering (SERS) spectroscopy,[8,9] to the extent that Raman scattering signal due to a single molecule can be detected.[10,11] In addition to enhancing spectroscopic signals, optical excitation of plasmon resonances can drive surface photochemistry of adsorbates.[12−18] These dual plasmonic effects inherently combine surface reactions and in situ detection of reactant and product species, providing a convenient platform for mechanistic investigation of heterogeneous catalysis. While plasmon-enhanced spectroscopy such as SERS is relatively well established,[19−21] plasmon-driven photochemical reaction is a growing area of research.

The mechanism of plasmon-driven surface photochemical reactions has mainly been discussed in terms of hot charge carriers that result from the nonradiative decay of plasmon resonances.[22−24] This mechanism involves transfer of the energetic electrons to the adsorbed chemical species and is expected to depend on the surface−molecule adsorption geometry and orbital hybridization with the surface. Examples of plasmon-driven reactions that are believed to be initiated by hot electron transfer to an unoccupied orbital of adsorbate include H_2 dissociation.[25] Recent theoretical modeling shows that the antibonding molecular orbital of the H_2 that hybridizes with a gold nanoparticle lies about 1.5 eV above the Fermi energy of the metal, indicating the feasibility of particle−molecule charge transfer.[26] Since the potential energy surface of the antibonding orbital is repulsive, the charge transfer can lead to dissociation of the molecule. Other examples of plasmon-driven chemical reactions that may involve hot electron transfer include ethylene epoxidation,[27] azo-coupling of self-assembled *para*-aminothiophenol (PATP)[28−34] and *para*-nitrothiophenol (PNTP),[35−40] conversion of PNTP to PATP[41] and vice versa,[42] esterification of

Received: December 14, 2018
Revised: February 10, 2019
Published: February 18, 2019

DOI: 10.1021/acs.jpcc.8b12054
J. Phys. Chem. C 2019, 123, 8469−8483

aldehydes,[43] and CO_2 reduction.[44,45] Except the H_2 dissociation and CO_2 reduction, the other reactions are believed to involve oxygen that can be activated by the energetic plasmon electrons.[27,32,34] That is, for the most part, the hot electron transfer mechanism may result in the formation of surface-bound transient anionic species such as H^-, O_2^-, or CO_2^-. Interestingly, the formation of these species is well-known from gas-phase studies.[46−49] In the gas phase, metastable anions can be stabilized through solvation,[50−52] while interaction with the nanoparticle surface and coadsorbates such as water and oxygen molecules can have a similar stabilizing effect.

Vibrational signatures of anionic radicals resulting from plasmon electron transfer to bipyridine have also been observed recently.[53] Furthermore, cis−trans isomerization of 1,2-bis(4-pyridyl)ethylene on gold nanosphere oligomers has been attributed to hot-electron-driven photochemistry.[54] In another study, plasmon-driven cross-linking and carbonaceous reaction of self-assembled organic molecules have been shown to have similarity with surface chemistry induced by secondary electrons of high-energy electron-beam and X-ray radiation.[55] There are also a large number of notable earlier examples of plasmon-driven photochemical reactions[56−62] reported following the discovery of SERS.[63,64]

Photochemistry on resonantly excited plasmonic nanostructures can also be initiated via plasmon-pumped electronic excitation of adsorbed molecules provided that the pumping rate competes with the rate of energy transfer back to the metal surface.[65,66] It has been suggested that intersystem crossing to triplet states that have relatively long lifetime can reduce the competition of nonradiative processes.[67] Recently, the photochemical conversion of methylene blue (MB) to thionine on plasmonic gold nanoparticles has been shown to depend on excitation wavelength, indicating the importance of plasmon-pumped electronic excitation of the MB adsorbate.[68,69] Similarly, the photodissociation of $(CH_3S)_2$ on Ag(111) and Cu(111) surfaces is believed to be initiated by near-field enhanced direct electronic excitation of the reactant.[70,71] It may also be difficult to rule out the role of plasmon-pumped electronic excitation of reactants in other interesting wavelength-dependent plasmon-driven photochemical transformations[72] considering that electronic transition energy shift and spectral broadening[73−75] can create uncertainty to determine the overlap of the reactant absorption band with the plasmon resonance at the excitation wavelength.

In addition to localized energy and hot electrons, the dephasing of surface plasmons generates a local heating effect[76−81] that can assist the surface photochemistry. In general, all the effects of plasmon excitation (near-field, hot carriers, and thermal) need to be considered in mechanistic investigation of photochemistry on resonantly photoexcited plasmonic metal nanoparticles. While there is significant effort in quantifying hot carriers and thermal contributions to plasmon-driven photochemical reactions, experimental results that demonstrate the importance of plasmon-pumped (near-field enhanced) electronic excitation of adsorbates remain scarce. The importance of charge transfer versus energy transfer is expected to depend on the surface molecule adsorption geometry and the overlap of the excitation wavelength with the resonances of the nanoparticle and the molecule adsorbed on the nanoparticle.

In this article, the relevance of hot electron transfer and plasmon-pumped adsorbate excitation in plasmon-driven reaction mechanisms is discussed based on the photochemistry of PATP[42] and MB.[68,69] The article is organized as follows. In Section 2, the branching of PATP photochemical transformation depending on the presence of cetyltrimethylammonium bromide (CTAB) surface ligand that facilitates hot carrier separation will be discussed. In Section 3, plasmon-enhanced N-demethylation of MB will be presented to demonstrate the importance of resonant excitation of adsorbate states as well as atmospheric and adsorption conditions. The conclusion and future outlook are provided in Section 4.

2. LIGAND-MEDIATED HOT-ELECTRON-INDUCED BRANCHING REACTION

In a conventional sense of heterogeneous catalysis, surface ligands are expected to reduce the reactivity of the catalyst by blocking the active sites.[82−87] The role of surface ligands in plasmon-driven surface photochemistry can depend on the interaction of the surface ligand with the charge carriers. In particular, surface-bound halides that interact with the positive charge are expected to enhance the interaction of the hot electrons with the reactant of interest.[88]

We have studied the surface ligand effect by comparing the photochemistry of PATP adsorbed in three different interfaces as displayed in the schematics in Figure 1a−c.[42] In Figure 1a, the

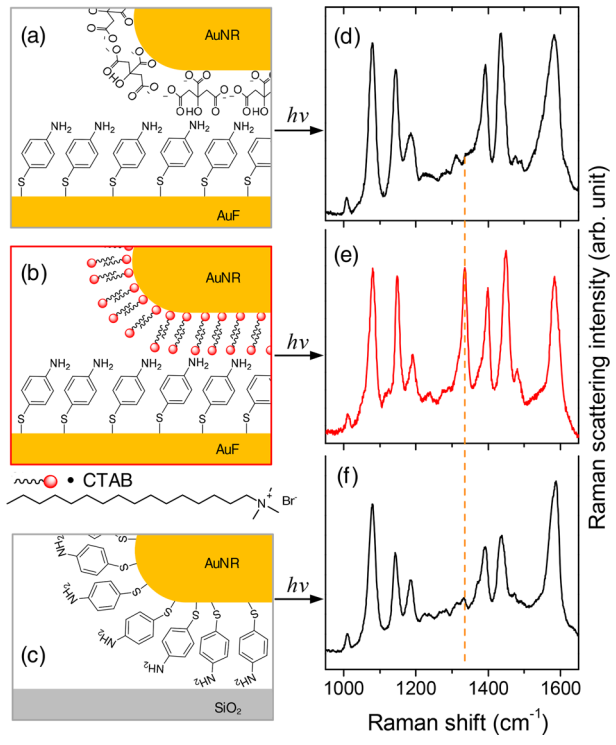

Figure 1. Effect of surface ligand. (a, d) When the PATP molecules are self-assembled on gold film and AuNRs with a citrate surface ligand are placed on top (a), vibrational frequencies characteristic of DMAB are observed (d). (b, e) When AuNRs with CTAB surface ligand are used (b), a strong vibration peak (due to N−O stretch) is observed at 1328 cm^{-1} (e). (c, f) The N−O peak is absent when the PATP molecules are self-assembled on the AuNRs replacing CTAB. Adapted with permission from ref 42. Copyright (2017) American Chemical Society.

PATP molecules are self-assembled on gold film and gold nanorods (AuNRs) with citrate surface ligands placed on top. The vibrational bands observed in the SERS spectrum (Figure 1d) for this sample are consistent with reported spectra obtained on roughened silver surfaces[28] and on citrate-coated silver and gold

DOI: 10.1021/acs.jpcc.8b12054
J. Phys. Chem. C 2019, 123, 8469−8483

nanoparticles.[29,31,32,89−91] The vibrational bands at 1143, 1392, and 1437 cm^{-1} are characteristic of the *p*,*p*′-dimercaptoazobenzene (DMAB) product[28,29,92] formed via an oxidative coupling reaction of self-assembled PATP molecules,[32,34] while the peaks at 1080 and 1580 cm^{-1} can be due to both PATP and DMAB.[28,29,92] When the surface ligand is changed to CTAB for nominally the same size of AuNRs (40 nm diameter and 80 nm length), a new prominent peak is observed at 1328 cm^{-1} in addition to the vibrational signatures of DMAB, as shown in Figure 1e. The peak at 1328 cm^{-1} can be assigned to N−O vibration, and it indicates the oxidation of PATP to PNTP. In contrast, when the PATP molecules are directly adsorbed on the AuNRs by replacing the CTAB surface ligands, the N−O vibrational band has completely disappeared as shown in Figure 1f.[42]

CTAB bound to gold nanoparticles has a characteristic Raman scattering peak at ∼180 cm^{-1} due to Au−Br stretching vibration frequency,[93−95] which can be used to confirm the correlation between CTAB content and PNTP product signal. As shown in Figure 2a, strong relative intensity of the N−O peak at 1328 cm^{-1} is accompanied by a strong Au−Br peak at 180 cm^{-1}. On the other hand, as seen in Figure 2b, when the PATP molecules are directly adsorbed on the AuNRs by replacing CTAB, the N−O peak is completely absent, which is consistent with the absence of the Au−Br peak at 180 cm^{-1}. The 1328 cm^{-1} peak frequency, assigned to N−O stretching frequency, is in very good agreement with the N−O vibrational frequency of solid PNTP as can be seen comparing Figures 2a and 2c. Clearly, the strong correlation between the Au−Br and the N−O vibrational bands underscores the role of CTAB in converting PATP to PNTP.

The mechanism of plasmon-driven oxidation of PATP to PNTP in the presence of CTAB may be similar to the mechanism of the reverse reaction (reduction of PNTP to PATP) on silver nanoparticles in acidic solution in the presence of halide counterions (Cl^-, Br^-, and I^-).[88] In both cases, the photochemical reactions are likely initiated by hot electron transfer to chemisorbed species. That is, the reaction can be initiated by electron transfer to O_2 in the case of PATP oxidation[32,34] and electron transfer to H^+ in the case of PNTP reduction.[88] After the electron is transferred to the adsorbed species, the halide anions can react with the positive charge on the metal surface, thereby minimizing the rate of electron return to the surface and increasing the number of hot electrons available to activate oxygen molecules.[27,32,88] Electron transfer to molecular oxygen can produce O_2^- superoxide that is strongly adsorbed to the surface of the nanoparticles.[32,96] The conversion of PATP to DMAB and PNTP possibly involves the same initial step, that is, reaction of the superoxide with the NH_2 group of PATP.[32,96] In the photocatalytic oxidation of aniline on Pt nanoparticles supported on TiO_2, nitrosobenzene and azobenzene have been detected.[96] According to the mechanism proposed by Konaka et al.,[97] the formation of the azobenzene should involve a reaction between the nitrosobenzene product and unreacted aniline that may be at very low number density depending on the concentration of charge carriers. The mechanism of plasmon-driven oxidation of PATP should be similar, and high concentration of hot electrons preferentially leads to the formation of PNTP as opposed to DMAB. As a result, branching photochemical reactions can take place as shown by Scheme 1.

In summary, the transformation of PATP on AuNRs exclusively to DMAB in the absence of CTAB on the AuNRs and to a mixture of DMAB and PNTP in the presence of CTAB indicates hot-electron-driven reaction mechanism. It is important to note

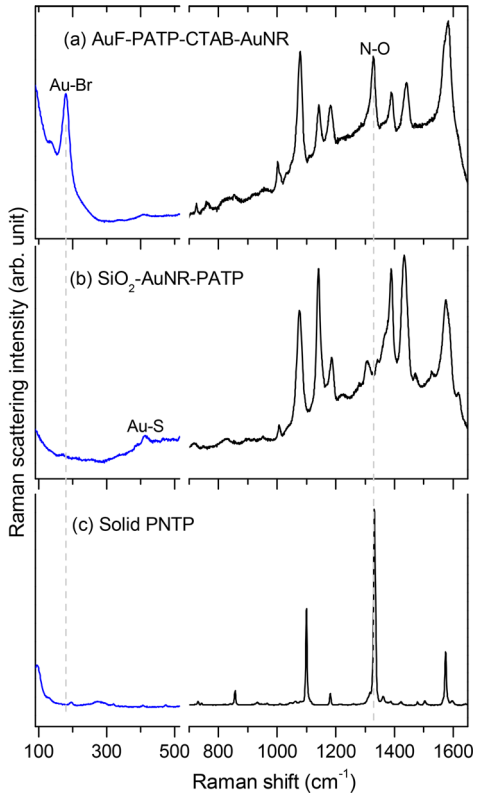

Figure 2. Correlation between CTAB content on the AuNRs and the N−O signal. (a) Strong Au−Br vibration band at 180 cm^{-1} correlates with strong intensity of the N−O vibration band at 1328 cm^{-1} for CTAB-coated AuNRs placed on PATP self-assembled on gold film (AuF). (b) The PATP is assembled on the AuNRs replacing CTAB resulting in the absence of Au−Br and N−O vibration bands. (c) Regular Raman spectrum of solid PNTP. All the results are obtained at λ = 633 nm. Adapted with permission from ref 42. Copyright (2017) American Chemical Society.

Scheme 1. Branching Reaction Pathways for Plasmon-Driven Oxidation of PATP

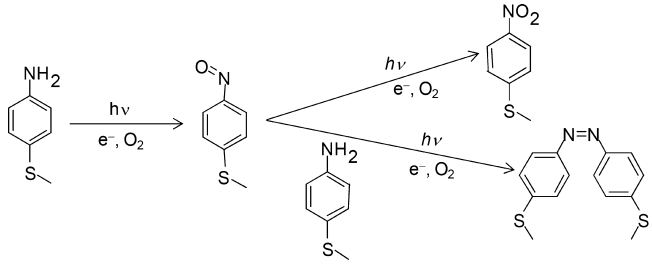

that changing surface ligands can change a number of variables in the reaction including the distance between the plasmonic surfaces, counterion concentration, surface charge, and carrier lifetime.[98,99] For the specific reaction of PATP to PNTP oxidation, the distance effect may be ruled out based on the comparison of the results in Figures 1a and 1b assuming that citrate and CTAB surface ligands provide approximately similar separations. The influence of CTAB can be explained in terms of counterion and surface charge that appears to increase the lifetime of the hot electron for the reaction.

3. PLASMON-PUMPED ADSORBATE EXCITATION AND PHOTOCHEMISTRY

When particle plasmon resonances spectrally overlap with the electronic transition energy of molecules adsorbed on the

DOI: 10.1021/acs.jpcc.8b12054
J. Phys. Chem. C 2019, 123, 8469−8483

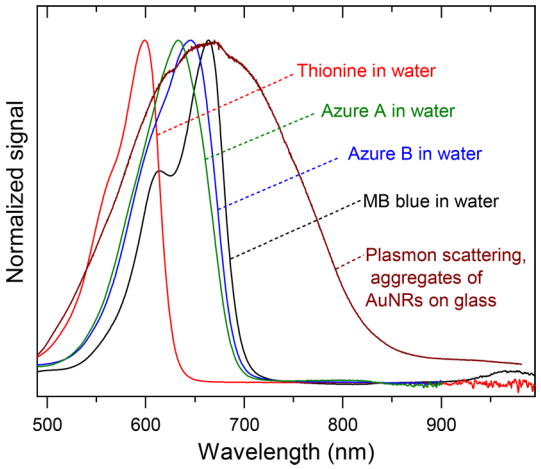

Figure 3. Spectral overlap of the molecular and plasmon resonances. The absorption spectra of MB, azure B, azure A, and thionine in water and the plasmon scattering spectrum of AuNRs (Diameter 40 nm and length 90 nm) as aggregated on coverslip glass.

nanoparticles, the adsorbate experiences enhanced rate of electron transition from its highest occupied molecular orbital (HOMO) to the lowest unoccupied molecular orbital (LUMO) due to the high mode density of the plasmon surface field.[100−103]

This plasmon-pumped electronic excitation of adsorbates can initiate important photochemistry at photon flux comparable to that of the solar radiation. Here, we highlight this mechanism using plasmon-enhanced N-demethylation of methylene blue (PEND-MB) on plasmonic gold nanoparticles as model reactions in which MB is converted to thionine and other partial N-demethylation products (azures A, B, C).[68,69] As shown in Figure 3, the absorption bands of aqueous solutions of MB and its N-demethylated derivatives appear in the visible spectral region. The scattering spectrum shown by the brown line in Figure 3 shows that the plasmon resonances of AuNRs (~40 nm diameter and ~90 nm length) aggregated on glass overlap with the absorption bands of MB and its derivatives. Adsorption of molecules on metal surfaces is expected to induce peak energy shift and line width broadening to an extent that depends on the nature of the surface−molecule interaction.[73−75]

For MB and its N-demethylated derivatives on the gold surface, the surface−molecule interaction is dominated by weak dispersion forces as recent theoretical calculations indicate.[104] Consistent with the physisorption nature of the interaction, the peak positions in the SERS spectra agree very closely with the corresponding peak positions in the regular Raman spectra of the solid powders as shown in Figure 4. The spectra presented in Figure 4 are obtained at 633 nm excitation wavelength, and the SERS signals for MB and its derivatives (azure B, azure A, and

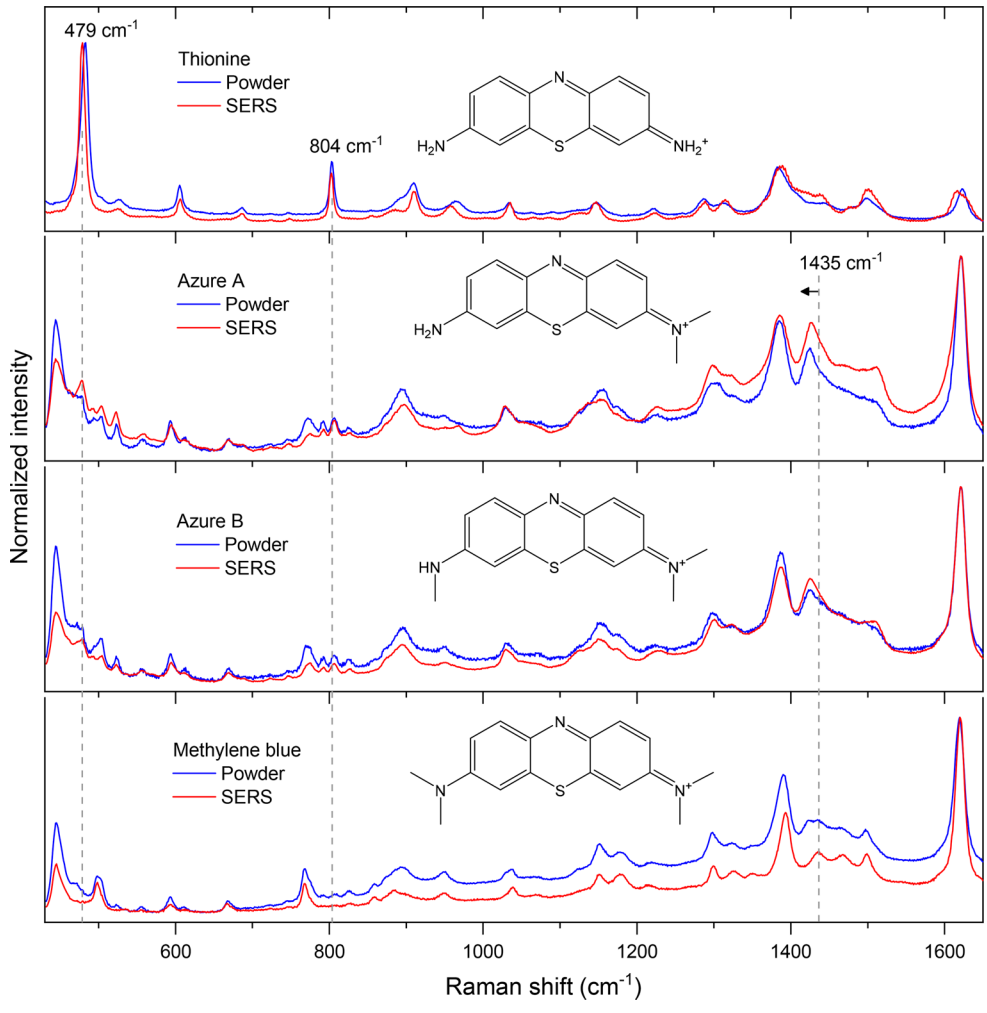

Figure 4. Normal Raman spectra of solid powders (blue lines) and SERS spectra (red lines) of methylene blue, azure B, azure A, and thionine as labeled.

DOI: 10.1021/acs.jpcc.8b12054
J. Phys. Chem. C 2019, 123, 8469−8483

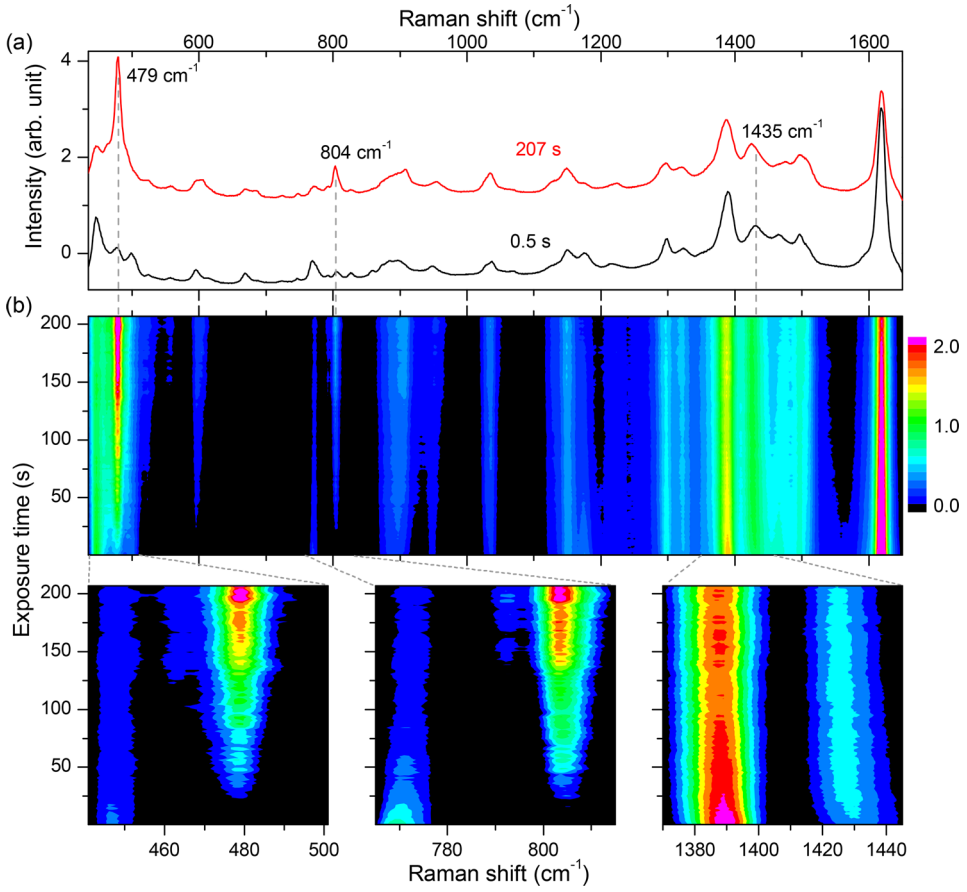

Figure 5. Temporal evolution of SERS spectra demonstrating PEND-MB. (a) Representative SERS spectra recorded in ambient atmosphere at the beginning (black line) and after 200 s of illumination using 633 nm excitation wavelength. (b) Intensity map representing 400 spectra acquired sequentially during illumination for about 207 s. The zoom-in intensity maps at the bottom show the important spectral changes with time. Each spectrum is recorded with 0.5 s acquisition time at 0.4 mW incident power focused with 0.7 NA objective.

thionine) are comparably strong suggesting similar contribution of molecular resonance effects as the spectral broadening upon adsorption can lead to the overlap of the excitation wavelength with the absorption bands for all the adsorbates. As a result, the reactant and product species can be monitored with high sensitivity by taking advantage of the large SERS cross-section that results from resonance Raman and electromagnetic enhancement effects.[105−108]

In the discussion of PEND-MB photochemical reaction, the spectra presented in Figure 4 will be used as reference. The prominent peaks at 479 and 804 cm^{-1} in the thionine spectrum can be used to quantify the conversion of MB to thionine. Similarly, the downshift of the 1435 cm^{-1} peak will be used to ascertain partial N-demethylation of MB.

The temporal evolution of the MB SERS spectra obtained under continuous illumination at 633 nm excitation wavelength in ambient atmosphere is shown in Figure 5. The prominent changes can be observed by comparing the spectra recorded at 0.5 and 200 s exposure times as shown in Figure 5a. The intensity map (Figure 5b) that represents 400 spectra acquired sequentially shows the appearance of new vibrational bands as a function of exposure time. Referring to the spectra presented in Figure 4, the spectral changes can be interpreted as follows.[68,69] (1) The new peak that appears at 479 cm^{-1} can be assigned to the skeletal deformation mode of thionine product. (2) The new peak at 804 cm^{-1} can be assigned to the NH_2 rocking vibration that requires complete N-demethylation at least at one of the N-terminals. (3) The red-shift from the 1435 cm^{-1} initial peak position can be attributed to partial N-demethylation products that include azure B, azure A, and azure C. We note that the prominent vibrational bands at 479 and 804 cm^{-1} are completely absent in the MB spectrum (see Figure 4), providing high contrast of reactant and product signals.

Insight into the mechanism of the PEND-MB can be obtained by performing the experiment under different excitation, atmospheric, and adsorption conditions as summarized next.

3.1. Excitation Wavelength Dependence. Our hypothesis that the photochemical conversion of MB to thionine on gold nanostructures is driven by plasmon-pumped electronic excitation can be tested by detuning the plasmon resonance and excitation energy away from the HOMO−LUMO transition energy of MB. To this end, the SERS spectra obtained at 633 nm excitation wavelength have been compared to that obtained at 532 and 808 nm excitation wavelengths such that the excitation energy overlaps with the plasmon resonances but not with the electronic transition energy of MB.[68] In Figure 6a, the dark-field scattering spectra of gold nanospheres (AuNSs, 40 nm diameter) and AuNRs (40 nm width and 148 nm length) incubated in MB solution and aggregated on oxide-coated silicon wafer are presented. The plasmon resonance of aggregates of AuNSs are excited more efficiently with the 532 nm laser than with the 633 nm due to more significant spectral overlap with the former. Similarly, the plasmon resonances of the AuNRs are excited more appreciably with the 808 nm laser than with the 633 nm. The data presented in

DOI: 10.1021/acs.jpcc.8b12054
J. Phys. Chem. C 2019, 123, 8469−8483

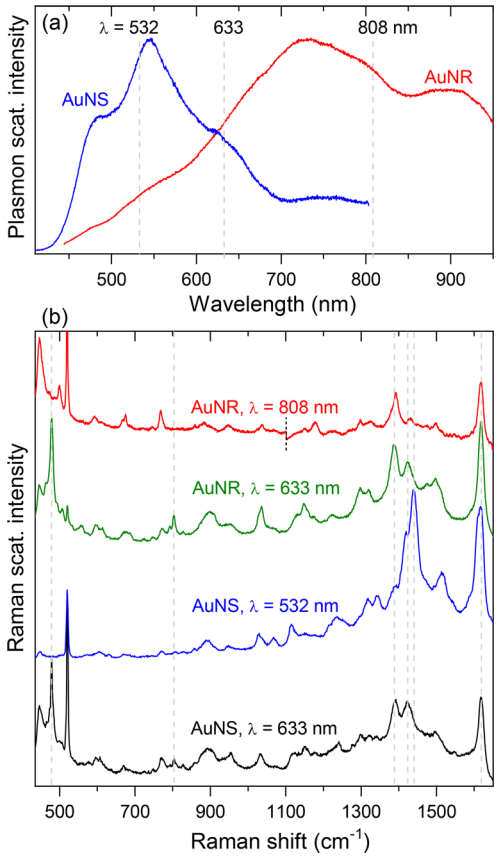

Figure 6. Excitation wavelength and plasmon resonance effects. (a) Dark-field scattering spectra of aggregates of gold nanospheres (AuNSs, diameter 40 nm) (blue line) and gold nanorods (AuNRs, 40 nm × 148 nm) (red line) functionalized with MB and deposited on a silica surface. (b) SERS spectra of MB adsorbed on the AuNSs and AuNRs recorded 30 s after continuous exposure to the excitation lasers. The peak at 520 cm^{-1} is due to silicon. Adapted with permission from ref 68. Copyright (2017) American Chemical Society.

Figure 6b show that PEND-MB occurs when a 633 nm excitation source is used for both plasmonic systems as indicated by the appearance of the prominent vibrational signatures of thionine (the peaks at 479 and 804 cm^{-1}). In contrast, no N-demethylation reaction is observed when 532 and 808 nm lasers are used regardless of the more efficient excitation of the plasmon resonances than at 633 nm. It is important to note that if the dominant reaction mechanism involves hot electron transfer the N-demethylation reaction would have been observed at 532 nm and/or 808 nm lasers which are expected to give more efficient excitation of the plasmon resonances.

In addition to the appearance or absence of the peaks at 479 and 804 cm^{-1} depending on the excitation wavelengths, notable differences can be observed in the 1360−1560 cm^{-1} region comparing the SERS spectra obtained at 532 and 633 nm excitation wavelengths as can be seen in Figure 6b. At 532 nm, the intensity at 1435 cm^{-1} is much higher than the intensity at 1392 cm^{-1}, whereas the opposite trend is observed at 633 nm excitation. The spectral pattern at 633 nm can be attributed to partial N-demethylation (referring to Figure 4), while understanding the relative intensity pattern observed at 532 nm requires further investigations.

Although they have been wrongly assigned to methylene blue, vibrational signatures of thionine are evident in some published SERS spectra of MB adsorbed on silver surface at 532 nm excitation wavelengths.[109−111] The discrepancy on gold versus silver surfaces may originate from the different adsorption properties of MB on gold and silver surfaces.[104] Depending on the nature of the surface−molecule interactions on different surfaces, the absorption band of the adsorbate can shift, resulting in different degrees of spectral overlap with the excitation wavelength on gold and silver surfaces. Surface ligands, counterions, and solvent molecules can also influence the adsorption properties as well as charge-transfer processes.

3.2. Excitation of Adsorbate on Nonplasmonic Surface. Excitation of MB adsorbed on nonplasmonic surfaces using 633 nm excitation laser line that overlaps with the electronic transition energy of MB does not lead to N-demethylation.[68] An example is shown in Figure 7, where the Raman

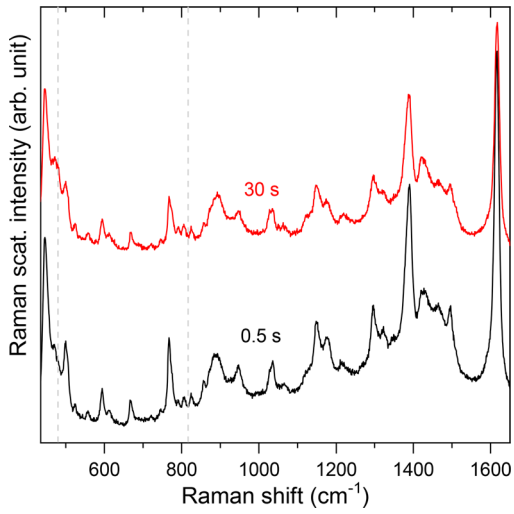

Figure 7. Raman spectra of MB adsorbed on gold film in the absence of plasmonic nanoparticles. The gold substrate was kept inside 1.5 × 10^{-5} M MB in ethanol solution overnight, and the substrate was not washed as it was pulled out of the solution so that thicker than a monolayer of MB sample was obtained to improve the signal-to-noise ratio. The spectra were recorded with acquisition time of 1 s at the 633 nm excitation wavelength with excitation intensity of ∼100 kW/cm^2. Adapted with permission from ref 68. Copyright (2017) American Chemical Society.

spectra of MB adsorbed on bulk gold film (∼50 thick) remain essentially the same upon continuous illumination regardless of the incident excitation intensity. The spectra in Figure 7 were acquired at irradiation intensity of ∼100 000 W/cm^2 at which no N-demethylation of MB was observed. In contrast, on optically excited plasmonic gold nanostructures, the photochemical reaction is observed at incident laser intensity as low as 100 W/cm^2. This observation underscores the importance of the intense local field to pump the electronic excitation of the adsorbate at very low incident photon flux. The observations in Figures 6 and 7 indicate that excitation of both the molecular and the plasmon resonances are important to induce the N-demethylation of methylene blue on the gold surface.

3.3. Atmospheric Conditions. The results on the PEND-MB discussed so far are obtained at ambient conditions. Mechanistic understanding of the reaction requires determining all the reactants that include gaseous species such as oxygen. To this end, the photochemical reaction has been carried out under controlled atmospheric conditions.[69] The temporal evolutions of the spectra obtained at different atmospheric conditions are compared in Figure 8. Under ambient air and oxygen

DOI: 10.1021/acs.jpcc.8b12054
J. Phys. Chem. C 2019, 123, 8469−8483

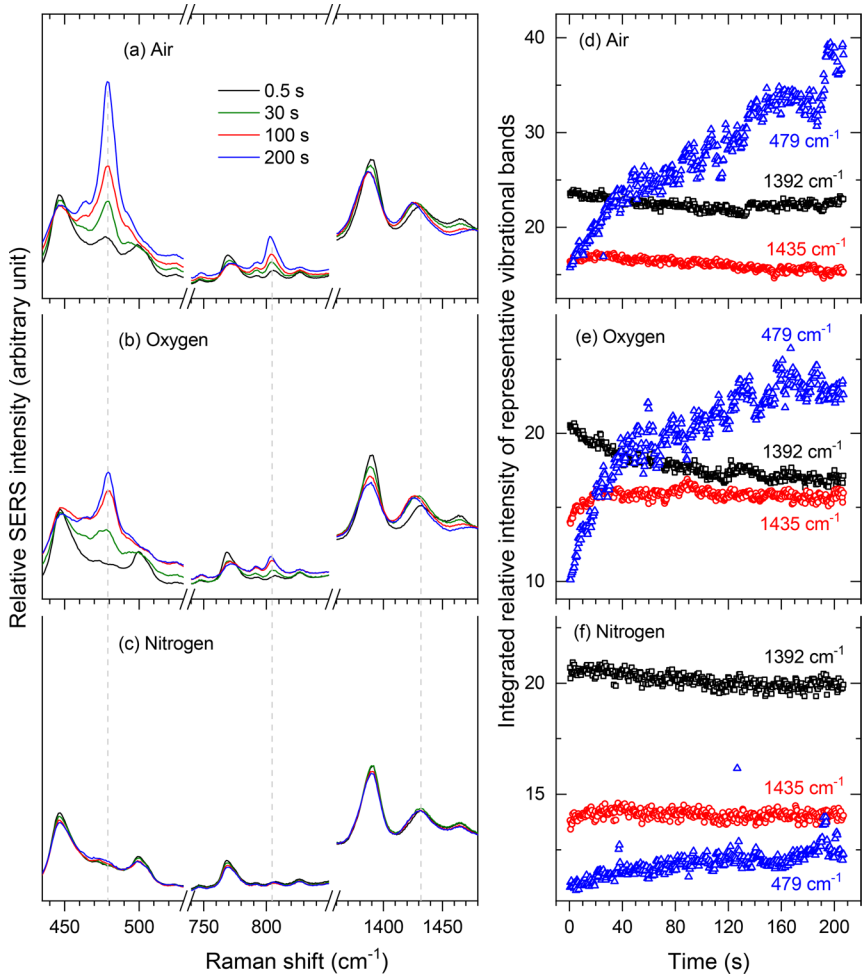

Figure 8. Temporal evolution of the SERS signal of MB adsorbed on AuNRs and illuminated with 0.4 mW of 633 nm CW laser (focused with 0.7 NA objective) in air (a, d), oxygen (b, e), and nitrogen (c, f) atmospheres. The SERS spectra are acquired continuously with 0.5 s acquisition time for over 200 s of continuous illumination, and the black, green, red, and blue lines in (a)−(c) represent average spectra of at least 10 different spots on the same sample at different exposure times, as labeled. (d)−(f) Integrated intensities of representative vibrational bands plotted as a function of exposure time. Adapted with permission from ref 69. Copyright (2018) American Chemical Society.

atmosphere, continuous exposure of the sample results in the appearance and growth of the vibrational bands at 479 and 804 cm^{-1} (Figures 8a and 8b). In contrast, in a nitrogen atmosphere, the intensities at the corresponding peak positions are within the background level as can be seen in Figure 8c. These observations indicate that oxygen is involved in the PEND-MB reaction. The integrated intensities of representative vibrational bands are plotted as a function of exposure time as shown in Figures 8d−f. As can be seen in Figures 8d,e, the intensity of thionine product signal increases with time and becomes higher than that of the 1392 cm^{-1} band, which is used as a reference because of its comparable intensity in both MB and thionine spectra, after about 40 s in the reactive atmospheres. In the inert (nitrogen) atmosphere, the relative intensity at the 479 cm^{-1} band remains within the background level during the continuous illumination of the sample (Figure 8f), confirming that conversion of MB to thionine is negligible in the absence of oxygen.

In addition to the appearance of prominent new peaks at 479 and 804 cm^{-1}, the vibrational mode that initially peaks at 1435 cm^{-1} red-shifts with increasing exposure time, and the shift is accompanied by a relative intensity increase depending on the atmospheric condition. This vibrational mode has been assigned to the in-plane NCH bending vibration of MB[112] and, therefore, should disappear upon complete N-demethylation of MB (thionine formation) as can be seen in Figure 4. Hence, the frequency red-shift and intensity rise with exposure time can be attributed to partial N-demethylation products that include azure B, azure A, and azure C, which is consistent with the reference spectra shown in Figure 4.

For more quantitative analysis of the partial N-demethylation, the integrated intensities and frequency shifts of the representative bands are plotted in Figure 9. In air and oxygen atmospheres, the relative intensity of the 1435 cm^{-1} band increases with exposure time, while that of the other bands remains nearly constant in air and decreases slightly in oxygen as shown in Figures 9a,b. For the band that initially peaks at ∼1435 cm^{-1}, the intensity rise is accompanied by significant frequency red-shift depending on the atmospheric conditions as shown in Figure 9d−f. Within 120 s exposure time, red-shifts of about 5 and 3 cm^{-1} are observed in reactive and inert atmospheres, respectively. Again, based on the reference spectra presented in Figure 4, the frequency shift is attributed to partial N-demethylation of MB. The shift in the nitrogen atmosphere indicates non-negligible reaction possibly due to the presence of trace amounts of oxygen as adsorbates.

DOI: 10.1021/acs.jpcc.8b12054
J. Phys. Chem. C 2019, 123, 8469−8483

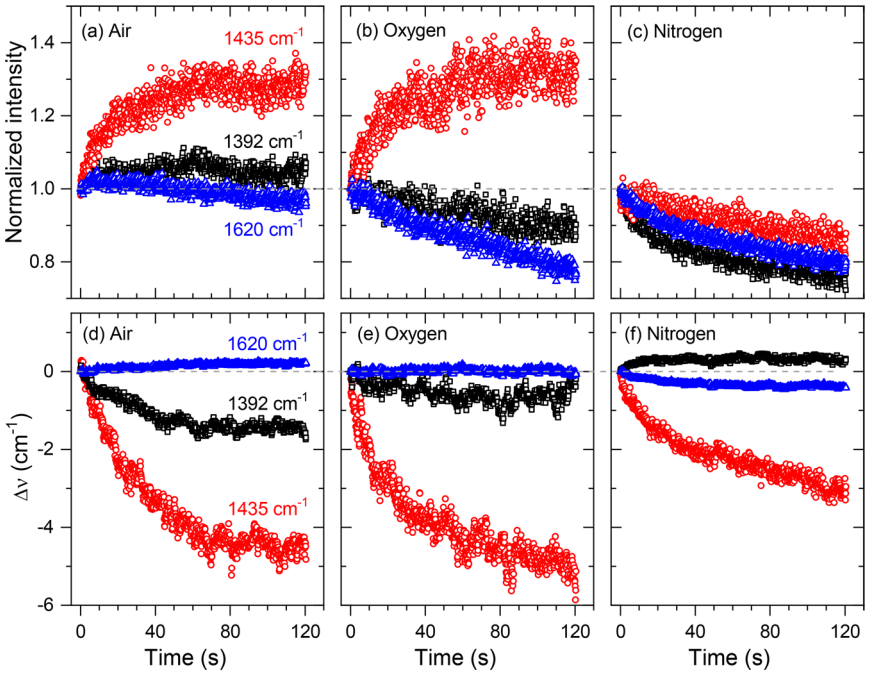

Figure 9. (a)−(c) Integrated and normalized relative intensities of representative vibrational bands plotted as a function of irradiation time in (a) air, (b) oxygen, and (c) nitrogen atmospheres. (d)−(f) Vibrational frequency shift of the different bands as labeled based on the initial peak frequencies. The vibrational frequencies are determined by fitting a Gaussian function to the spectra. The integrated intensities and frequencies are extracted from 1000 spectra each recorded with 0.1 s acquisition time within 120 s of continuous irradiation time using 0.2 mW of 633 nm CW laser that is focused with a 0.7 NA objective. Adapted with permission from ref 69. Copyright (2018) American Chemical Society.

3.4. Surface−Molecule Proximity. Comparing the spectra shown by the black and green lines in Figure 6b (obtained using the same excitation wavelength), it can be seen that the 1424 cm^{-1} to 1392 cm^{-1} peak intensity ratio is higher for MB adsorbed on gold spheres with citrate surface ligand (black lines) than that on AuNRs with CTAB surface ligand (green line). This observation suggests that the adsorption on gold spheres favors partial N-demethylation as can be inferred based on the patterns in reference spectra provided in Figure 4. To obtain further evidence, the SERS properties of MB adsorbed directly on the bare gold surface prepared using electron-beam evaporation (MB-Au) are compared with that obtained by adsorbing on similarly prepared gold nanostructures coated with a monolayer of poly(sodium 4-styrenesulfonate) (MB-PSS-Au) as shown in Figure 10. For the MB-Au sample, two peaks at 1421 and 1435 cm^{-1} are observed, and the relative intensity of the former increases with exposure time. For the MB-PSS-Au sample, the 1421 cm^{-1} peak has shifted to ~1426 cm^{-1}, and its relative intensity increases with exposure time. Based on the results presented in Figure 4, the 1426 cm^{-1} peak position can be assigned to azure B or C, and the red shift to 1421 cm^{-1} for the MB-Au sample can be attributed to surface−molecule interaction because of direct coupling to the gold surface.

As shown in Figure 10b, the intensity ratio of the 1421 cm^{-1} to 1392 cm^{-1} peaks for the MB-Au sample (open circles) is higher than the corresponding peak intensity ratio for the MB-PSS-Au sample (solid circles). On the other hand, the intensity ratio of 479 cm^{-1} to 446 cm^{-1} peaks is higher for the MB-PSS-Au sample (solid triangles) than for the MB-Au sample (open triangles), indicating that the conversion of MB to thionine is favored in the presence of PSS. The observation of stronger thionine product signal in the presence of PSS may indicate optimal surface−molecule proximity to minimize competing radiative and nonradiative processes as predicted by Nitzan and Brus.[66] In other words, it can be argued that the trend observed in Figure 10 supports our proposed mechanism that involves plasmon-pumped HOMO−LUMO electronic transition. However, the PSS may also influence the charge carrier separation and their lifetimes.

3.5. Hydration Effect: "Wet" Versus "Dry" Adsorbate. When aqueous solution of MB and gold nanoparticles is drop-casted and dried, MB is likely adsorbed in its hydrated form,[113−115] and the water molecules can be involved in the photochemical N-demethylation. Indeed, when the water content is reduced by suspending the molecules and the nanoparticles in ethanol solvent, PEND-MB is drastically reduced as summarized in Figure 11. Comparing the relative intensity of the bands at 479 and 804 cm^{-1} in Figure 11a (obtained under a flow of oxygen over *dehydrated* surface−molecule complex) to the corresponding intensities in Figure 8b (obtained under the flow of oxygen over *hydrated* surface−molecule complex), it can be seen that the PEND-MB reaction is suppressed when the surface−molecule complex is dehydrated. When the experiment is repeated after introducing water molecules in the gas phase by expanding oxygen gas through a water bubbler, the vibrational signatures of thionine still remain weak as shown in Figure 11b. The peak intensities plotted in Figure 11c,d show that the relative intensity of the 479 cm^{-1} band remains significantly lower than the intensity of the 1392 cm^{-1} band throughout the exposure time. This trend is in contrast to that observed in Figures 8d and e, where the relative intensity of the 479 cm^{-1} band becomes larger than that of the 1392 cm^{-1} band with increasing time. In addition, the frequency shift for the mode that peaks at 1435 cm^{-1} is negligible, suggesting that partial N-demethylation is also suppressed in the absence of water. The fact that the vibrational signatures of N-demethylation remain weak even in the presence of water molecules in the gas phase suggests that it is hydrated MB that undergoes N-demethylation reaction. In hydrated MB, water molecules can be the source of hydrogen atoms that replaces the methyl groups.

DOI: 10.1021/acs.jpcc.8b12054
J. Phys. Chem. C 2019, 123, 8469−8483

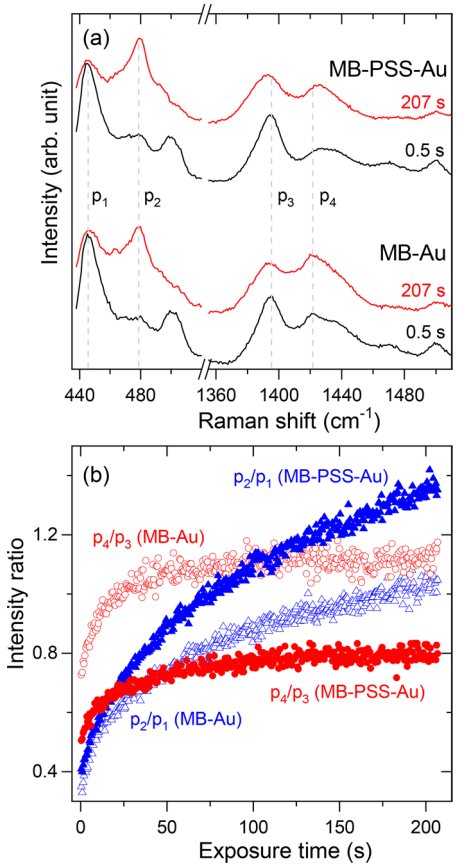

Figure 10. Spacer layer effect. (a) Representative spectra showing the relative intensities of the peaks labeled p_1−p_4 at the beginning (black line) and end (red line) of illumination at 633 nm for 207 s in the presence (upper two spectra) and absence (lower two spectra) of poly(sodium 4-styrenesulfonate) (PSS) coating on e-beam evaporated gold nanostructures as labeled. Each spectrum represents an average of at least 10 different spots on the same sample. (b) Peak intensity ratios as a function of exposure time. Adapted with permission from ref 69. Copyright (2018) American Chemical Society.

3.6. Singlet Oxygen. It is well-known that singlet oxygen ($^1O_2$) reacts with organic molecules, resulting in oxidative transformation and degradation.[116,117] Thermally or photon-induced generation of singlet oxygen is used to initiate oxidative N-dealkylation reactions.[118,119] Selective biocatalytic oxidative N-demethylation reactions are known to play a crucial role in nucleic acid regulation and synthesis.[120−123] More recently, highly selective biomimetic riboflavin-catalyzed oxidative demethylation of *N*-methyl adenine and related compounds using blue light has been reported by Xie and coauthors.[124] Photoexcited adsorbed molecular oxygen via hot electron transfer is proposed to initiate the oxidation of dyes and simple organic molecules such as formaldehyde, ethylene, and methanol under ambient conditions.[125] In this mechanism, hot electrons are injected into the antibonding molecular orbital of adsorbed O_2 to form electronically excited adsorbed O_2^-. The superoxide relaxes quickly to the ground electronic but vibrationally excited state of neutral O_2 by releasing electrons back into the metal. The activated neutral oxygen undergoes fast reaction to yield selective oxidation of organic molecules that are very close to the surface of the metal nanoparticles. Alternatively, adsorbed O_2 captures hot electron to form very reactive anionic oxygen that readily extracts protons from the organic molecules or water to generate more reactive free radical species to initiate the oxidation reaction.[118,119] Furthermore, recent experimental observations indicate that plasmonic nanoparticles enhance the efficiency of photosensitizers to generate singlet oxygen.[126−128] Considering that MB is a well-known photosensitizer,[129] the photochemical N-demethylation is likely to involve singlet oxygen. In fact, it has been shown that singlet oxygen drives N-demethylation of different organic molecules.[130−133]

The interaction of MB with visible light can induce electronic transition from the singlet ground state (S_0) to the singlet excited state (S_1) that can be followed by intersystem crossing to the excited triplet state (T_1) as illustrated in Figure 12. The energy transfer from MB (T_1) to oxygen in its triplet ground state ($^3O_2$) can generate the reactive singlet oxygen ($^1O_2$). That is, the plasmon field drives the photochemical N-demethylation by pumping the $S_0 \rightarrow S_1$ electronic excitation of the MB adsorbate that leads to enhanced generation of $^1O_2$.

Singlet oxygen can interact with MB to form a charge-transfer complex (exciplex).[134,135] Similar to the solution-phase mechanism,[131] H atom transfer within the complex can lead to formation of a radical species, which in the presence of water results in N-demethylation as shown in Scheme 2,[69] in which only one of the methyl groups is shown for simplicity, where Z^+ represents the rest of the cationic structural constituents of MB including the fused ring system and the two methyl groups attached to the N atom on the other end of the molecule.

3.7. Transfer and Solvation of Hot Electron. The discussion so far, particularly the dependence on excitation wavelength (Section 3.1), strongly supports that photochemical conversion of MB to thionine on gold nanoparticles is initiated by plasmon-pumped electronic excitation of the adsorbate. However, based on these observations, we cannot rule out the involvement of hot electron transfer in the reaction. Signatures of light-induced surface molecule interaction and partial charge transfer processes can be revealed by analyzing the frequencies of the vibrational modes that may be sensitive to charge redistribution in the surface−molecule complex. In the oxygen atmosphere, the frequency shift due to surface−molecule interaction and charge transfer can be overwhelmed by chemical transformation. However, the charging effect can be discovered in N_2 atmosphere, in which the photochemical reaction is suppressed.

As shown in Figure 9f, in N_2 atmosphere, the 1392 and 1620 cm^{-1} vibration modes shift in opposite direction, indicating the importance of light-induced surface−molecule interaction and charge-transfer effects. The surface−molecule interaction may cause delocalization of the π-electron density of the fused aromatic ring. This charge delocalization can strengthen the 1392 cm^{-1} vibration mode, which is due to the stretching vibration of the C−N attached to the methyl groups coupled to the stretching vibration of the fused aromatic ring. In contrast, the 1620 cm^{-1} ring vibration mode can be softened as the electron density is pulled from the aromatic system.[136]

We note that the blue-shifting of the 1392 cm^{-1} vibration frequency in inert atmosphere (Figure 9f) is in contrast to the red-shifting in the reactive atmospheres (Figures 9d and 9e), which suggests that the charge transfer and the N-demethylation reaction shift the vibration frequency in opposite direction. On the other hand, from the shifting of the vibrational frequency that initially appears at 1435 cm^{-1}, it is clear that the photochemical N-demethylation is not completely absent. These observations suggest that if the photochemical transformation could be suppressed completely, the shifts induced by the surface−molecule interaction and charge transfer for the bands

DOI: 10.1021/acs.jpcc.8b12054
J. Phys. Chem. C 2019, 123, 8469−8483

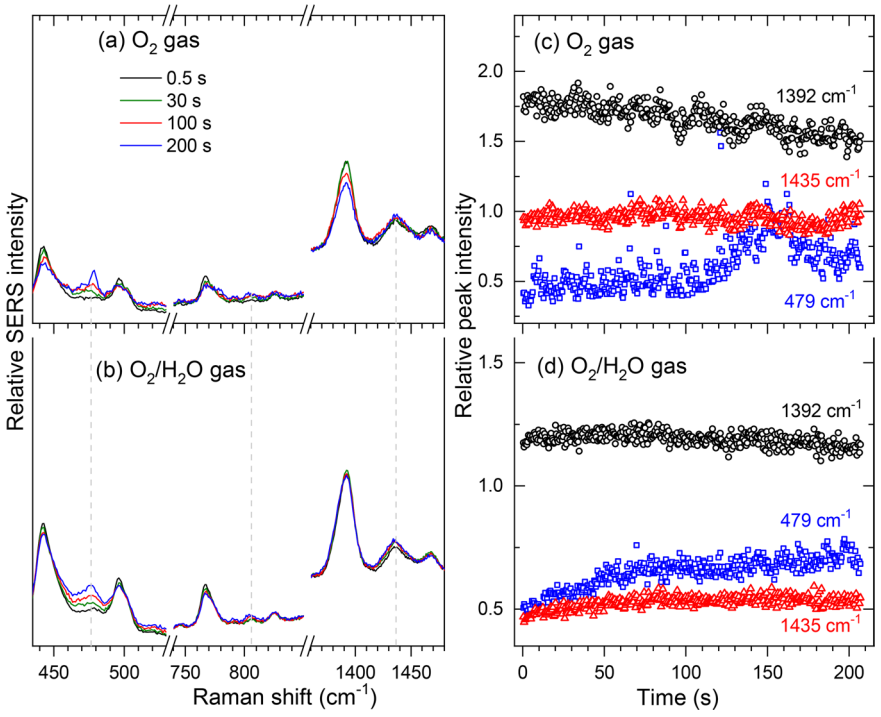

Figure 11. Temporal evolution of the SERS signal for the dehydrated MB−AuNR complex. The amount of adsorbed water is minimized by using ethanol solution of MB and AuNRs during the sample preparation. Representative spectra acquired under the flow of (a) dry O_2 gas and (b) O_2/H_2O gas formed by passing the O_2 gas through a water bubbler. (c, d) Relative peak intensities extracted from the spectra acquired under the flow of (c) dry O_2 gas and (d) O_2/H_2O gas. Adapted with permission from ref 69. Copyright (2018) American Chemical Society.

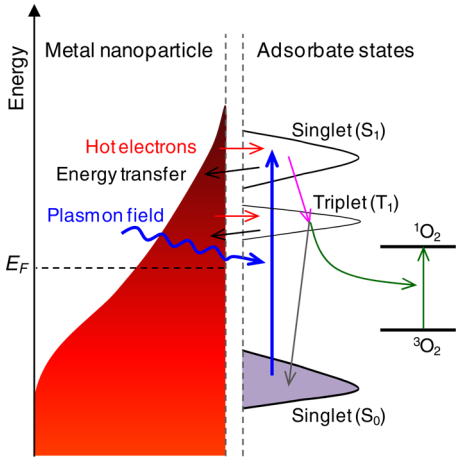

Figure 12. Schematic showing possible photophysical processes for MB on gold nanoparticles when the excitation energy is in resonance with the particle plasmon resonance and MB adsorbate electronic transition. The plasmon near field of the particle pumps the $S_0 \rightarrow S_1$ electronic transition of the MB adsorbate (blue lines). S_1 to T_1 intersystem crossing (purple arrow) can populate the MB T_1 state, from which energy transfer (green arrows) can promote oxygen from its triplet ground state ($^3O_2$) to singlet excited state ($^1O_2$). The black arrows indicate energy transfer to the metal surface, and red arrows indicate hot electron transfer to the unoccupied adsorbate states. Adapted with permission from ref 69. Copyright (2018) American Chemical Society.

that initially peak at 1392 and 1620 cm^{-1} might be more significant than observed in Figure 9f. More insight into the charge transfer effect may be obtained by performing the SERS experiment at excitation wavelengths that do not induce photochemical transformation (see Section 3.1). In fact, hot

Scheme 2. Proposed Reaction Pathway of PEND-MB

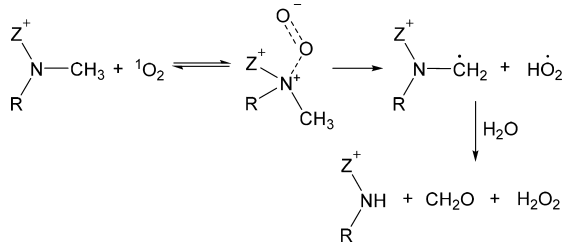

electron transfer to the unoccupied orbital of MB adsorbed on silver nanocubes has been proposed based on the unusually large anti-Stokes to Stokes Raman intensity ratio at 785 nm excitation wavelength at which no N-demethylation has been observed.[110,111]

Charge transfer to MB adsorbate and local heating due to dissipation of energy from the resonant excitation of the molecule and particle resonances may assist the photochemical reactions by activating the surface−molecule complex to readily undergo chemical transformation. In addition, the hot electron can assist the reaction by activating molecular oxygen.[27,32,34] The formation of singlet oxygen and hot electron transfer can take place in concert. Considering the involvement of water in the reaction, it may be appropriate to think in terms of solvated hot electron, where a metastable $[MB(O_2)_m(H_2O)_n]^-$ cluster anion is adsorbed on the gold surface. This charge transfer process can modify the mechanism in Scheme 2 according to the pathways proposed for photochemical N-demethylation of ruflox-acin.[133] It is also important to note that the photochemical transformation of MB to thionine involves multistep reactions to replace four methyl groups with hydrogen. As a result, confirming whether the excited-state processes are important at each step requires future systematic experimental studies.

DOI: 10.1021/acs.jpcc.8b12054
J. Phys. Chem. C 2019, 123, 8469−8483

4. SUMMARY AND FUTURE OUTLOOK

The experimental results summarized in this article indicate that photochemistry can be induced on optically excited plasmonic nanostructures by hot plasmon electron transfer to an unoccupied orbital of the adsorbate and/or by plasmon-pumped HOMO−LUMO electron transition of the adsorbate. The importance of hot electron transfer and plasmon-pumped adsorbate excitation is expected to vary depending on many factors that include adsorption geometry, surface-molecule energy−level alignment, and spectral overlap between the resonances of the nanoparticle and the adsorbate, surface ligands and coadsorbed solvent molecules, and ionic species. The fact that plasmon excitation drives chemical reaction and enhances spectroscopic signals simultaneously can be exploited to improve our understanding of heterogeneous catalysis in general. Currently, mechanistic understanding of plasmon-driven surface reaction is at its infancy. Concerted experimental and theoretical efforts are needed. Recent experimental advances indicate windows of opportunity to tackle the problem. SERS can be used to detect reactant and product species.[68,69] Tip-based near-field optical microscopy can map near-field distribution[4,137,138] and Raman scattering[37,139−141] in real space with high spatial resolution. These super-resolution capabilities can be combined to correlate plasmon-field localization with reactivity because with continual improvements of the tip-based microscopy it may be possible to resolve the distribution of the reactant and product species adsorbed on individual plasmonic nanoparticles. For example, a recent report by Apkarian and co-workers demonstrates the possibility of imaging electrostatic fields with submolecular spatial resolution using tip-enhanced Raman scattering for imaging charge density distribution on single metalloporphyrins adsorbed on Au(111).[142] Similarly, scanning tunneling microscopy can be used to visualize reaction and charge density on surfaces.[71,143,144] Technical advances for probing thermal effects are also improving.[78,79,81,145] The electronic absorption band of molecules adsorbed on metal surfaces is largely unknown despite its critical importance for understanding the role of plasmon-pumped electronic excitation in plasmon-driven photochemistry. Plasmon-enhanced electronic excitation of organic adsorbates can lead to generation of singlet oxygen. Keeping in mind that most examples of plasmon-driven photochemistry are carried out in oxygen atmosphere, the role of singlet oxygen can be more prevalent than currently thought. The generation of singlet oxygen is likely accompanied by immediate hot plasmon electron transfer and formation of cluster anion considering the reactivity of singlet oxygen. Formation of adsorbed transient cluster anions can increase the lifetime of hot electrons, making them available for driving chemical reactions.

■ AUTHOR INFORMATION

Corresponding Author

*Terefe G. Habteyes: habteyes@unm.edu.

ORCID

Terefe G. Habteyes: 0000-0001-5978-6464

Author Contributions

The manuscript was written through contributions of all authors. All authors have given approval to the final version of the manuscript.

Notes

The authors declare no competing financial interest.

Biographies

Tefera E. Tesema is a PhD graduate student in the Department of Chemistry and Chemical Biology, University of New Mexico, working in Habteyes' research group. He received his bachelor and master's degrees in chemistry from Addis Ababa University, Ethiopia. His research interest is focused on the fundamental understanding of plasmonic metal nanoparticles, plasmon-driven photochemistry, and semiconductor quantum dots.

Bijesh Kafle is a PhD candidate in Habteyes' research group in the Department of Chemistry and Chemical Biology at the University of New Mexico. He received his BS (2008) and MS (2010) in chemistry from Tribhuvan University Nepal. His research is focused on understanding the physical properties of semiconductor and plasmonic nanoparticles, self-assembly of excitonic and plasmonic nanoparticles, plasmon-enhanced photochemistry, and scattering-type near-field optical microscopy.

Terefe Habteyes is an associate professor in the Department of Chemistry and Chemical Biology and member of the Center for High

DOI: 10.1021/acs.jpcc.8b12054
J. Phys. Chem. C 2019, 123, 8469−8483

Technology Materials at the University of New Mexico (UNM). He received his BS (1997) and MS (2000) both in Chemistry from Addis Ababa University, Ethiopia. He did his graduate study (2002–2008) at the University of Arizona working with Prof. Andrei Sanov on the development of time-of-flight mass spectrometry coupled to velocity map imaging for investigating gas-phase photochemistry. From 2008 to 2012, he worked on the development of near-field scanning optical microscopy as well as on the design, fabrication, and characterization of plasmonic materials as a University of California President's postdoctoral fellow working at UC Berkeley and the Molecular Foundry, Lawrence Berkeley National Lab, under the supervision of Profs. Leone and Alivisatos. He began his faculty position at UNM in August 2012. His research interests include super-resolution near-field optical imaging, nanoplasmonics, nanophotonics, photochemistry, and plasmon-enhanced surface spectroscopy.

■ ACKNOWLEDGMENTS

This research has been supported by the U.S. National Science Foundation Grant No. 1651478 and the U.S. Air Force Office of Scientific Research Grant No. FA9550-18-1-0512.

■ ABBREVIATIONS

SERS, surface-enhanced Raman scattering; PATP, *para*-aminothiophenol; PNTP, *para*-nitrothiophenol; DMAB, *p,p′*-dimercaptoazobenzene; CTAB, cetyltrimethylammonium bromide; MB, methylene blue; PEND-MB, plasmon-enhanced N-demethylation of MB

■ REFERENCES

(1) Sarid, D.; Challener, W. *Modern Introduction to Surface Plasmons*; University Press: Cambridge, UK, 2010.
(2) Willets, K. A.; Van Duyne, R. P. Localized Surface Plasmon Resonance Spectroscopy and Sensing. *Annu. Rev. Phys. Chem.* **2007**, *58*, 267–297.
(3) Jain, P. K.; Huang, W. Y.; El-Sayed, M. A. On the Universal Scaling Behavior of the Distance Decay of Plasmon Coupling in Metal Nanoparticle Pairs: A Plasmon Ruler Equation. *Nano Lett.* **2007**, *7*, 2080–2088.
(4) Kiesow, K. I.; Dhuey, S.; Habteyes, T. G. Mapping Near-Field Localization in Plasmonic Optical Nanoantennas with 10 nm Spatial Resolution. *Appl. Phys. Lett.* **2014**, *105*, No. 053105.
(5) Maier, S. A. Plasmonic Field Enhancement and SERS in the Effective Mode Volume Picture. *Opt. Express* **2006**, *14*, 1957–1964.
(6) Xu, H. X.; Aizpurua, J.; Kall, M.; Apell, P. Electromagnetic Contributions to Single-Molecule Sensitivity in Surface-Enhanced Raman Scattering. *Phys. Rev. E: Stat. Phys., Plasmas, Fluids, Relat. Interdiscip. Top.* **2000**, *62*, 4318–4324.
(7) Stockman, M., Electromagnetic Theory of Sers. In *Surface-Enhanced Raman Scattering*; Kneipp, K., Moskovits, M., Kneipp, H., Eds.; Springer: Berlin Heidelberg, 2006; Vol. *103*, pp 47–65.
(8) Moskovits, M. Surface-Enhanced Spectroscopy. *Rev. Mod. Phys.* **1985**, *57*, 783–826.
(9) Otto, A.; Mrozek, I.; Grabhorn, H.; Akemann, W. Surface-Enhanced Raman-Scattering. *J. Phys.: Condens. Matter* **1992**, *4*, 1143–1212.
(10) Nie, S.; Emory, S. R. Probing Single Molecules and Single Nanoparticles by Surface-Enhanced Raman Scattering. *Science* **1997**, *275*, 1102–1106.
(11) Kneipp, K.; Wang, Y.; Kneipp, H.; Perelman, L. T.; Itzkan, I.; Dasari, R. R.; Feld, M. S. Single Molecule Detection Using Surface-Enhanced Raman Scattering (SERS). *Phys. Rev. Lett.* **1997**, *78*, 1667.
(12) Linic, S.; Aslam, U.; Boerigter, C.; Morabito, M. Photochemical Transformations on Plasmonic Metal Nanoparticles. *Nat. Mater.* **2015**, *14*, 567–576.
(13) Zhang, Z. L.; Xu, P.; Yang, X. Z.; Liang, W. J.; Sun, M. T. Surface Plasmon-Driven Photocatalysis in Ambient, Aqueous and High-Vacuum Monitored by SERS and TERS. *J. Photochem. Photobiol., C* **2016**, *27*, 100–112.
(14) Kim, M.; Lin, M.; Son, J.; Xu, H. X.; Nam, J. M. Hot-Electron-Mediated Photochemical Reactions: Principles, Recent Advances, and Challenges. *Adv. Opt. Mater.* **2017**, *5*, 1700004.
(15) Zhang, Y.; He, S.; Guo, W.; Hu, Y.; Huang, J.; Mulcahy, J. R.; Wei, W. D. Surface-Plasmon-Driven Hot Electron Photochemistry. *Chem. Rev.* **2018**, *118*, 2927–2954.
(16) Kazuma, E.; Kim, Y. Mechanistic Studies of Plasmon Chemistry on Metal Catalysts. *Angew. Chem., Int. Ed.* **2019**, *58*, 2–11.
(17) Brongersma, M. L.; Halas, N. J.; Nordlander, P. Plasmon-Induced Hot Carrier Science and Technology. *Nat. Nanotechnol.* **2015**, *10*, 25–34.
(18) Liu, J. G.; Zhang, H.; Link, S.; Nordlander, P. Relaxation of Plasmon-Induced Hot Carriers. *ACS Photonics* **2018**, *5*, 2584–2595.
(19) Stiles, P. L.; Dieringer, J. A.; Shah, N. C.; Van Duyne, R. R. Surface-Enhanced Raman Spectroscopy. *Annu. Rev. Anal. Chem.* **2008**, *1*, 601–626.
(20) Kneipp, K.; Moskovits, M.; Kneipp, H. *Topics in Applied Physics*; Springer: Germany, 2006; Vol. *103*.
(21) Le Ru, E.; Etchegoin, P. *Principles of Surface-Enhanced Raman Spectroscopy*; Elsevier: Amsterdam, The Netherlands, 2009.
(22) Govorov, A. O.; Zhang, H.; Gun'ko, Y. K. Theory of Photoinjection of Hot Plasmonic Carriers from Metal Nanostructures into Semiconductors and Surface Molecules. *J. Phys. Chem. C* **2013**, *117*, 16616–16631.
(23) Sundararaman, R.; Narang, P.; Jermyn, A. S.; Goddard, W. A.; Atwater, H. A. Theoretical Predictions for Hot-Carrier Generation from Surface Plasmon Decay. *Nat. Commun.* **2014**, DOI: 10.1038/ncomms6788.
(24) Manjavacas, A.; Liu, J. G.; Kulkarni, V.; Nordlander, P. Plasmon-Induced Hot Carriers in Metallic Nanoparticles. *ACS Nano* **2014**, *8*, 7630–7638.
(25) Mukherjee, S.; Libisch, F.; Large, N.; Neumann, O.; Brown, L. V.; Cheng, J.; Lassiter, J. B.; Carter, E. A.; Nordlander, P.; Halas, N. J. Hot Electrons Do the Impossible: Plasmon-Induced Dissociation of H_2 on Au. *Nano Lett.* **2013**, *13*, 240–247.
(26) Zhang, Y.; Nelson, T.; Tretiak, S.; Guo, H.; Schatz, G. C. Plasmonic Hot-Carrier-Mediated Tunable Photochemical Reactions. *ACS Nano* **2018**, *12*, 8415–8422.
(27) Christopher, P.; Xin, H. L.; Linic, S. Visible-Light-Enhanced Catalytic Oxidation Reactions on Plasmonic Silver Nanostructures. *Nat. Chem.* **2011**, *3*, 467–472.
(28) Huang, Y.-F.; Zhu, H.-P.; Liu, G.-K.; Wu, D.-Y.; Ren, B.; Tian, Z.-Q. When the Signal Is Not from the Original Molecule to Be Detected: Chemical Transformation of Para-Aminothiophenol on Ag During the Sers Measurement. *J. Am. Chem. Soc.* **2010**, *132*, 9244–9246.
(29) Fang, Y. R.; Li, Y. Z.; Xu, H. X.; Sun, M. T. Ascertaining P,P'-Dimercaptoazobenzene Produced from P-Aminothiophenol by Selective Catalytic Coupling Reaction on Silver Nanoparticles. *Langmuir* **2010**, *26*, 7737–7746.
(30) Yan, X. F.; Wang, L. Z.; Tan, X. J.; Tian, B. Z.; Zhang, J. L. Surface-Enhanced Raman Spectroscopy Assisted by Radical Capturer for Tracking of Plasmon-Driven Redox Reaction. *Sci. Rep.* **2016**, DOI: 10.1038/srep30193.
(31) Choi, H. K.; Shon, H. K.; Yu, H.; Lee, T. G.; Kim, Z. H. B(2) Peaks in Sers Spectra of 4-Aminobenzenethiol: A Photochemical Artifact or a Real Chemical Enhancement? *J. Phys. Chem. Lett.* **2013**, *4*, 1079–1086.
(32) Huang, Y. F.; Zhang, M.; Zhao, L. B.; Feng, J. M.; Wu, D. Y.; Ren, B.; Tian, Z. Q. Activation of Oxygen on Gold and Silver Nanoparticles Assisted by Surface Plasmon Resonances. *Angew. Chem., Int. Ed.* **2014**, *53*, 2353–2357.
(33) Zhao, L. B.; Liu, X. X.; Zhang, M.; Liu, Z. F.; Wu, D. Y.; Tian, Z. Q. Surface Plasmon Catalytic Aerobic Oxidation of Aromatic Amines in Metal/Molecule/Metal Junctions. *J. Phys. Chem. C* **2016**, *120*, 944–955.
(34) Xu, P.; Kang, L. L.; Mack, N. H.; Schanze, K. S.; Han, X. J.; Wang, H. L. Mechanistic Understanding of Surface Plasmon Assisted Catalysis

DOI: 10.1021/acs.jpcc.8b12054
J. Phys. Chem. C 2019, 123, 8469–8483

on a Single Particle: Cyclic Redox of 4-Aminothiophenol. *Sci. Rep.* **2013**, *3*, 2997.
(35) Dong, B.; Fang, Y. R.; Xia, L. X.; Xu, H. X.; Sun, M. T. Is 4-Nitrobenzenethiol Converted to P,P '-Dimercaptoazobenzene or 4-Aminothiophenol by Surface Photochemistry Reaction? *J. Raman Spectrosc.* **2011**, *42*, 1205−1206.
(36) Dong, B.; Fang, Y. R.; Chen, X. W.; Xu, H. X.; Sun, M. T. Substrate-, Wavelength-, and Time-Dependent Plasmon-Assisted Surface Catalysis Reaction of 4-Nitrobenzenethiol Dimerizing to P,P '-Dimercaptoazobenzene on Au, Ag, and Cu Films. *Langmuir* **2011**, *27*, 10677−10682.
(37) Sun, M. T.; Zhang, Z. L.; Zheng, H. R.; Xu, H. X. In-Situ Plasmon-Driven Chemical Reactions Revealed by High Vacuum Tip-Enhanced Raman Spectroscopy. *Sci. Rep.* **2012**, DOI: 10.1038/srep00647.
(38) van Schrojenstein Lantman, E. M.; Deckert-Gaudig, T.; Mank, A. J. G.; Deckert, V.; Weckhuysen, B. M. Catalytic Processes Monitored at the Nanoscale with Tip-Enhanced Raman Spectroscopy. *Nat. Nanotechnol.* **2012**, *7*, 583−586.
(39) Kang, L. L.; Xu, P.; Zhang, B.; Tsai, H. H.; Han, X. J.; Wang, H. L. Laser Wavelength- and Power-Dependent Plasmon-Driven Chemical Reactions Monitored Using Single Particle Surface Enhanced Raman Spectroscopy. *Chem. Commun.* **2013**, *49*, 3389−3391.
(40) Choi, H.-K.; Park, W.-H.; Park, C.-G.; Shin, H.-H.; Lee, K. S.; Kim, Z. H. Metal-Catalyzed Chemical Reaction of Single Molecules Directly Probed by Vibrational Spectroscopy. *J. Am. Chem. Soc.* **2016**, *138*, 4673−4684.
(41) Joseph, V.; Engelbrekt, C.; Zhang, J. D.; Gernert, U.; Ulstrup, J.; Kneipp, J. Characterizing the Kinetics of Nanoparticle-Catalyzed Reactions by Surface-Enhanced Raman Scattering. *Angew. Chem., Int. Ed.* **2012**, *51*, 7592−7596.
(42) Kafle, B.; Poveda, M.; Habteyes, T. G. Surface Ligand-Mediated Plasmon-Driven Photochemical Reactions. *J. Phys. Chem. Lett.* **2017**, *8*, 890−894.
(43) Zhang, Y.; Xiao, Q.; Bao, Y.; Zhang, Y.; Bottle, S.; Sarina, S.; Zhaorigetu, B.; Zhu, H. Direct Photocatalytic Conversion of Aldehydes to Esters Using Supported Gold Nanoparticles under Visible Light Irradiation at Room Temperature. *J. Phys. Chem. C* **2014**, *118*, 19062−19069.
(44) Calaza, F.; Stiehler, C.; Fujimori, Y.; Sterrer, M.; Beeg, S.; Ruiz-Oses, M.; Nilius, N.; Heyde, M.; Parviainen, T.; Honkala, K.; et al. Carbon Dioxide Activation and Reaction Induced by Electron Transfer at an Oxide-Metal Interface. *Angew. Chem., Int. Ed.* **2015**, *54*, 12484−12487.
(45) Yu, S. J.; Wilson, A. J.; Heo, J.; Jain, P. K. Plasmonic Control of Multi-Electron Transfer and C-C Coupling in Visible-Light-Driven CO_2 Reduction on Au Nanoparticles. *Nano Lett.* **2018**, *18*, 2189−2194.
(46) Cooper, C. D.; Compton, R. N. Metastable Anions of CO_2. *Chem. Phys. Lett.* **1972**, *14*, 29−32.
(47) Celotta, R. J.; Bennett, R. A.; Levine, J.; Hall, J. L.; Siegel, M. W. Molecular Photodetachment Spectrometry 0.2. Electron Affinity of O_2 and Structure of O_2. *Phys. Rev. A: At., Mol., Opt. Phys.* **1972**, *6*, 631−642.
(48) Coe, J. V.; Snodgrass, J. T.; Freidhoff, C. B.; McHugh, K. M.; Bowen, K. H. Negative-Ion Photoelectron-Spectroscopy of the Negative Cluster Ion $H^-(NH_3)_1$. *J. Chem. Phys.* **1985**, *83*, 3169−3170.
(49) Kleingeld, J. C.; Ingemann, S.; Jalonen, J. E.; Nibbering, N. M. M. Formation of the NH_4^- Ion in the Gas-Phase. *J. Am. Chem. Soc.* **1983**, *105*, 2474−2475.
(50) Grumbling, E. R.; Sanov, A. Solvation Effects on Angular Distributions in $H^-(NH_3)_n$ and $NH_2^-(NH_3)_n$ Photodetachment: Role of Solute Electronic Structure. *J. Chem. Phys.* **2011**, *135*, 164301.
(51) Habteyes, T.; Velarde, L.; Sanov, A. Photodissociation of CO_2^- in Water Clusters Via Renner-Teller and Conical Interactions. *J. Chem. Phys.* **2007**, *126*, 154301.
(52) Akin, F. A.; Schirra, L. K.; Sanov, A. Photoelectron Imaging Study of the Effect of Monohydration on O_2^- Photodetachment. *J. Phys. Chem. A* **2006**, *110*, 8031−8036.
(53) Sprague-Klein, E. A.; McAnally, M. O.; Zhdanov, D. V.; Zrimsek, A. B.; Apkarian, V. A.; Seideman, T.; Schatz, G. C.; Van Duyne, R. P. Observation of Single Molecule Plasmon-Driven Electron Transfer in Isotopically Edited 4,4 '-Bipyridine Gold Nanosphere Oligomers. *J. Am. Chem. Soc.* **2017**, *139*, 15212−15221.
(54) Sprague-Klein, E. A.; Negru, B.; Madison, L. R.; Coste, S. C.; Rugg, B. K.; Felts, A. M.; McAnally, M. O.; Banik, M.; Apkarian, V. A.; Wasielewski, M. R.; et al. Photoinduced Plasmon-Driven Chemistry in Trans-1,2-Bis(4-Pyridyl)Ethylene Gold Nanosphere Oligomers. *J. Am. Chem. Soc.* **2018**, *140*, 10583−10592.
(55) Szczerbiński, J.; Gyr, L.; Kaeslin, J.; Zenobi, R. Plasmon-Driven Photocatalysis Leads to Products Known from E-Beam and X-Ray-Induced Surface Chemistry. *Nano Lett.* **2018**, *18*, 6740−6749.
(56) Goncher, G. M.; Harris, C. B. Enhanced Photofragmentation on a Silver Surface. *J. Chem. Phys.* **1982**, *77*, 3767−3768.
(57) Bunding, K. A.; Durst, R. A.; Bell, M. I. Surface-Enhanced Raman-Spectroscopy of N-Methylpyridinium Cation and Pyridine - Identification of Surface Species. *J. Electroanal. Chem. Interfacial Electrochem.* **1983**, *150*, 437−446.
(58) Goncher, G. M.; Parsons, C. A.; Harris, C. B. Photochemistry on Rough Metal-Surfaces. *J. Phys. Chem.* **1984**, *88*, 4200−4209.
(59) Lu, T.; Birke, R. L.; Lombardi, J. R. Surface Raman-Spectroscopy of the 3 Redox Forms of Methylviologen. *Langmuir* **1986**, *2*, 305−309.
(60) Sun, S. C.; Birke, R. L.; Lombardi, J. R.; Leung, K. P.; Genack, A. Z. Photolysis of Para-Nitrobenzoic Acid on Roughened Silver Surfaces. *J. Phys. Chem.* **1988**, *92*, 5965−5972.
(61) White, J. M. Photochemistry at Adsorbate Metal Interfaces - Issues and Examples. *J. Vac. Sci. Technol., B: Microelectron. Process. Phenom.* **1992**, *10*, 191−195.
(62) Suh, J. S.; Jang, N. H.; Jeong, D. H.; Moskovits, M. Adsorbate Photochemistry on a Colloid Surface: Phthalazine on Silver. *J. Phys. Chem.* **1996**, *100*, 805−813.
(63) Jeanmaire, D. L.; Vanduyne, R. P. Surface Raman Spectroelectrochemistry 0.1. Heterocyclic, Aromatic, and Aliphatic-Amines Adsorbed on Anodized Silver Electrode. *J. Electroanal. Chem. Interfacial Electrochem.* **1977**, *84*, 1−20.
(64) Moskovits, M. Surface-Roughness and Enhanced Intensity of Raman-Scattering by Molecules Adsorbed on Metals. *J. Chem. Phys.* **1978**, *69*, 4159−4161.
(65) Nitzan, A.; Brus, L. E. Can Photochemistry Be Enhanced on Rough Surfaces. *J. Chem. Phys.* **1981**, *74*, 5321−5322.
(66) Nitzan, A.; Brus, L. E. Theoretical-Model for Enhanced Photochemistry on Rough Surfaces. *J. Chem. Phys.* **1981**, *75*, 2205−2214.
(67) Wolkow, R. A.; Moskovits, M. Enhanced Photochemistry on Silver Surfaces. *J. Chem. Phys.* **1987**, *87*, 5858−5869.
(68) Tesema, T. E.; Kafle, B.; Tadesse, M. G.; Habteyes, T. G. Plasmon-Enhanced Resonant Excitation and Demethylation of Methylene Blue. *J. Phys. Chem. C* **2017**, *121*, 7421−7428.
(69) Tesema, T. E.; Annesley, C.; Habteyes, T. G. Plasmon-Enhanced Autocatalytic N-Demethylation. *J. Phys. Chem. C* **2018**, *122*, 19831−19841.
(70) Kazuma, E.; Jung, J.; Ueba, H.; Trenary, M.; Kim, Y. Direct Pathway to Molecular Photodissociation on Metal Surfaces Using Visible Light. *J. Am. Chem. Soc.* **2017**, *139*, 3115−3121.
(71) Kazuma, E.; Jung, J.; Ueba, H.; Trenary, M.; Kim, Y. Real-Space and Real-Time Observation of a Plasmon-Induced Chemical Reaction of a Single Molecule. *Science* **2018**, *360*, 521−525.
(72) Zhao, J.; Nguyen, S. C.; Ye, R.; Ye, B. H.; Weller, H.; Somorjai, G. A.; Alivisatos, A. P.; Toste, F. D. A Comparison of Photocatalytic Activities of Gold Nanoparticles Following Plasmonic and Interband Excitation and a Strategy for Harnessing Interband Hot Carriers for Solution Phase Photocatalysis. *ACS Cent. Sci.* **2017**, *3*, 482−488.
(73) Craighead, H. G.; Glass, A. M. Optical-Absorption of Small Metal Particles with Adsorbed Dye Coats. *Opt. Lett.* **1981**, *6*, 248−250.
(74) Darby, B. L.; Auguie, B.; Meyer, M.; Pantoja, A. E.; Le Ru, E. C. Modified Optical Absorption of Molecules on Metallic Nanoparticles at Sub-Monolayer Coverage. *Nat. Photonics* **2016**, *10*, 40−45.
(75) Birke, R. L.; Lombardi, J. R.; Saidi, W. A.; Norman, P. Surface-Enhanced Raman Scattering Due to Charge-Transfer Resonances: A

DOI: 10.1021/acs.jpcc.8b12054
J. Phys. Chem. C 2019, 123, 8469−8483

Time-Dependent Density Functional Theory Study of Ag_{13}-4-Mercaptopyridine. *J. Phys. Chem. C* **2016**, *120*, 20721−20735.
(76) Baffou, G.; Berto, P.; Bermúdez Ureña, E.; Quidant, R.; Monneret, S.; Polleux, J.; Rigneault, H. Photoinduced Heating of Nanoparticle Arrays. *ACS Nano* **2013**, *7*, 6478−6488.
(77) Yang, H.; He, L. Q.; Hu, Y. W.; Lu, X. H.; Li, G. R.; Liu, B. J.; Ren, B.; Tong, Y. X.; Fang, P. P. Quantitative Detection of Photothermal and Photoelectrocatalytic Effects Induced by SPR from Au@Pt Nanoparticles. *Angew. Chem., Int. Ed.* **2015**, *54*, 11462−11466.
(78) Yu, Y.; Sundaresan, V.; Willets, K. A. Hot Carriers versus Thermal Effects: Resolving the Enhancement Mechanisms for Plasmon-Mediated Photoelectrochemical Reactions. *J. Phys. Chem. C* **2018**, *122*, 5040−5048.
(79) Kamarudheen, R.; Castellanos, G. W.; Kamp, L. P. J.; Clercx, H. J. H.; Baldi, A. Quantifying Photothermal and Hot Charge Carrier Effects in Plasmon-Driven Nanoparticle Syntheses. *ACS Nano* **2018**, *12*, 8447−8455.
(80) Golubev, A. A.; Khlebtsov, B. N.; Rodriguez, R. D.; Chen, Y.; Zahn, D. R. T. Plasmonic Heating Plays a Dominant Role in the Plasmon-Induced Photocatalytic Reduction of 4-Nitrobenzenethiol. *J. Phys. Chem. C* **2018**, *122*, 5657−5663.
(81) Zhou, L. A.; Swearer, D. F.; Zhang, C.; Robatjazi, H.; Zhao, H. Q.; Henderson, L.; Dong, L. L.; Christopher, P.; Carter, E. A.; Nordlander, P.; et al. Quantifying Hot Carrier and Thermal Contributions in Plasmonic Photocatalysis. *Science* **2018**, *362*, 69−72.
(82) Haider, P.; Urakawa, A.; Schmidt, E.; Baiker, A. Selective Blocking of Active Sites on Supported Gold Catalysts by Adsorbed Thiols and Its Effect on the Catalytic Behavior: A Combined Experimental and Theoretical Study. *J. Mol. Catal. A: Chem.* **2009**, *305*, 161−169.
(83) Biswas, M.; Dinda, E.; Rashid, M. H.; Mandal, T. K. Correlation between Catalytic Activity and Surface Ligands of Monolayer Protected Gold Nanoparticles. *J. Colloid Interface Sci.* **2012**, *368*, 77−85.
(84) Ben-Shahar, Y.; Scotognella, F.; Waiskopf, N.; Kriegel, I.; Dal Conte, S.; Cerullo, G.; Banin, U. Effect of Surface Coating on the Photocatalytic Function of Hybrid CdS-Au Nanorods. *Small* **2015**, *11*, 462−471.
(85) Vu, K. B.; Bukhryakov, K. V.; Anjum, D. H.; Rodionov, V. O. Surface-Bound Ligands Modulate Chemoselectivity and Activity of a Bimetallic Nanoparticle Catalyst. *ACS Catal.* **2015**, *5*, 2529−2533.
(86) Ansar, S. M.; Kitchens, C. L. Impact of Gold Nanoparticle Stabilizing Ligands on the Colloidal Catalytic Reduction of 4-Nitrophenol. *ACS Catal.* **2016**, *6*, 5553−5560.
(87) Roy, S.; Roy, S.; Rao, A.; Devatha, G.; Pillai, P. P. Precise Nanoparticle−Reactant Interaction Outplays Ligand Poisoning in Visible-Light Photocatalysis. *Chem. Mater.* **2018**, *30*, 8415−8419.
(88) Xie, W.; Schlucker, S. Hot Electron-Induced Reduction of Small Molecules on Photorecycling Metal Surfaces. *Nat. Commun.* **2015**, DOI: 10.1038/ncomms8570.
(89) Huang, Y. Z.; Fang, Y. R.; Yang, Z. L.; Sun, M. T. Can P,P '-Dimercaptoazobisbenzene Be Produced from P-Aminothiophenol by Surface Photochemistry Reaction in the Junctions of a Ag Nanoparticle-Molecule-Ag (or Au) Film? *J. Phys. Chem. C* **2010**, *114*, 18263−18269.
(90) Sun, M. T.; Huang, Y. Z.; Xia, L. X.; Chen, X. W.; Xu, H. X. The pH-Controlled Plasmon-Assisted Surface Photocatalysis Reaction of 4-Aminothiophenol to P,P '-Dimercaptoazobenzene on Au, Ag, and Cu Colloids. *J. Phys. Chem. C* **2011**, *115*, 9629−9636.
(91) Wang, J. L.; Ando, R. A.; Camargo, P. H. C. Controlling the Selectivity of the Surface Plasmon Resonance Mediated Oxidation of P-Aminothiophenol on Au Nanoparticles by Charge Transfer from UV-Excited TiO_2. *Angew. Chem., Int. Ed.* **2015**, *54*, 6909−6912.
(92) Wu, D. Y.; Liu, X. M.; Huang, Y. F.; Ren, B.; Xu, X.; Tian, Z. Q. Surface Catalytic Coupling Reaction of P-Mercaptoaniline Linking to Silver Nanostructures Responsible for Abnormal Sers Enhancement: A DFT Study. *J. Phys. Chem. C* **2009**, *113*, 18212−18222.
(93) Nikoobakht, B.; El-Sayed, M. A. Surface-Enhanced Raman Scattering Studies on Aggregated Gold Nanorods. *J. Phys. Chem. A* **2003**, *107*, 3372−3378.
(94) Aguirre, C. M.; Kaspar, T. R.; Radloff, C.; Halas, N. J. CTAB Mediated Reshaping of Metallodielectric Nanoparticles. *Nano Lett.* **2003**, *3*, 1707−1711.
(95) Wang, H.; Levin, C. S.; Halas, N. J. Nanosphere Arrays with Controlled Sub-10 nm Gaps as Surface-Enhanced Raman Spectroscopy Substrates. *J. Am. Chem. Soc.* **2005**, *127*, 14992−14993.
(96) Shiraishi, Y.; Sakamoto, H.; Fujiwara, K.; Ichikawa, S.; Hirai, T. Selective Photocatalytic Oxidation of Aniline to Nitrosobenzene by Pt Nanoparticles Supported on Tio2 Under Visible Light Irradiation. *ACS Catal.* **2014**, *4*, 2418−2425.
(97) Konaka, R.; Kuruma, K.; Terabe, S. Mechanisms of Oxidation of Aniline and Related Compounds in Basic Solution. *J. Am. Chem. Soc.* **1968**, *90*, 1801−1806.
(98) Aruda, K. O.; Tagliazucchi, M.; Sweeney, C. M.; Hannah, D. C.; Schatz, G. C.; Weiss, E. A. Identification of Parameters through Which Surface Chemistry Determines the Lifetimes of Hot Electrons in Small Au Nanoparticles. *Proc. Natl. Acad. Sci. U. S. A.* **2013**, *110*, 4212−4217.
(99) Alvarez-Puebla, R. A.; Arceo, E.; Goulet, P. J. G.; Garrido, J. J.; Aroca, R. F. Role of Nanoparticle Surface Charge in Surface-Enhanced Raman Scattering. *J. Phys. Chem. B* **2005**, *109*, 3787−3792.
(100) Khurgin, J. B.; Sun, G.; Soref, R. A. Practical Limits of Absorption Enhancement Near Metal Nanoparticles. *Appl. Phys. Lett.* **2009**, *94*, No. 071103.
(101) Kinkhabwala, A.; Yu, Z. F.; Fan, S. H.; Avlasevich, Y.; Mullen, K.; Moerner, W. E. Large Single-Molecule Fluorescence Enhancements Produced by a Bowtie Nanoantenna. *Nat. Photonics* **2009**, *3*, 654−657.
(102) Lagos, N.; Sigalas, M. M.; Lidorikis, E. Theory of Plasmonic near-Field Enhanced Absorption in Solar Cells. *Appl. Phys. Lett.* **2011**, *99*, No. 063304.
(103) Itoh, T.; Yamamoto, Y. S.; Ozaki, Y. Plasmon-Enhanced Spectroscopy of Absorption and Spontaneous Emissions Explained Using Cavity Quantum Optics. *Chem. Soc. Rev.* **2017**, *46*, 3904−3921.
(104) Zhou, L.; Johnson, R.; Habteyes, T.; Guo, H. Adsorption of Methylene Blue and Its N-Demethylated Derivatives on the (111) Face of Coinage Metals: The Importance of Dispersion Interactions. *J. Chem. Phys.* **2017**, *146*, 164701.
(105) Hildebrandt, P.; Stockburger, M. Surface-Enhanced Resonance Raman-Spectroscopy of Rhodamine-6g Adsorbed on Colloidal Silver. *J. Phys. Chem.* **1984**, *88*, 5935−5944.
(106) Tognalli, N. G.; Fainstein, A.; Vericat, C.; Vela, M. E.; Salvarezza, R. C. Exploring Three-Dimensional Nanosystems with Raman Spectroscopy: Methylene Blue Adsorbed on Thiol and Sulfur Monolayers on Gold. *J. Phys. Chem. B* **2006**, *110*, 354−360.
(107) Lombardi, J. R.; Birke, R. L. A Unified Approach to Surface-Enhanced Raman Spectroscopy. *J. Phys. Chem. C* **2008**, *112*, 5605−5617.
(108) Morton, S. M.; Jensen, L. Understanding the Molecule-Surface Chemical Coupling in Sers. *J. Am. Chem. Soc.* **2009**, *131*, 4090−4098.
(109) Nicolai, S. H. A.; Rubim, J. C. Surface-Enhanced Resonance Raman (SERR) Spectra of Methylene Blue Adsorbed on a Silver Electrode. *Langmuir* **2003**, *19*, 4291−4294.
(110) Boerigter, C.; Campana, R.; Morabito, M.; Linic, S. Evidence and Implications of Direct Charge Excitation as the Dominant Mechanism in Plasmon-Mediated Photocatalysis. *Nat. Commun.* **2016**, *7*, 10545.
(111) Boerigter, C.; Aslam, U.; Linic, S. Mechanism of Charge Transfer from Plasmonic Nanostructures to Chemically Attached Materials. *ACS Nano* **2016**, *10*, 6108−6115.
(112) Dutta Roy, S. D.; Ghosh, M.; Chowdhury, J. Adsorptive Parameters and Influence of Hot Geometries on the SER(R)S Spectra of Methylene Blue Molecules Adsorbed on Gold Nanocolloidal Particles. *J. Raman Spectrosc.* **2015**, *46*, 451−461.
(113) Marr, H. E.; Stewart, J. M.; Chiu, M. F. Crystal-Structure of Methylene-Blue Pentahydrate. *Acta Crystallogr., Sect. B: Struct. Crystallogr. Cryst. Chem.* **1973**, *29*, 847−853.
(114) Rager, T.; Geoffroy, A.; Hilfiker, R.; Storey, J. M. D. The Crystalline State of Methylene Blue: A Zoo of Hydrates. *Phys. Chem. Chem. Phys.* **2012**, *14*, 8074−8082.

DOI: 10.1021/acs.jpcc.8b12054
J. Phys. Chem. C 2019, 123, 8469−8483

(115) Yan, S. H.; Zhang, H.; Yang, Z. B.; Tang, M. J.; Zhang, M. K.; Du, C. L.; Cui, H. L.; Wei, D. S. Transformation and Dehydration Kinetics of Methylene Blue Hydrates Detected by Terahertz Time-Domain Spectroscopy. *RSC Adv.* **2017**, *7*, 41667−41674.
(116) Li, H. R.; Wu, L. Z.; Tung, C. H. Reactions of Singlet Oxygen with Olefins and Sterically Hindered Amine in Mixed Surfactant Vesicles. *J. Am. Chem. Soc.* **2000**, *122*, 2446−2451.
(117) Bernstein, R.; Foote, C. S. Singlet Oxygen Involvement in the Photochemical Reaction of C-60 and Amines. Synthesis of an Alkyne-Containing Fullerene. *J. Phys. Chem. A* **1999**, *103*, 7244−7247.
(118) Zhu, H.; Chen, X.; Zheng, Z.; Ke, X.; Jaatinen, E.; Zhao, J.; Guo, C.; Xie, T.; Wang, D. Mechanism of Supported Gold Nanoparticles as Photocatalysts under Ultraviolet and Visible Light Irradiation. *Chem. Commun.* **2009**, 7524−7526.
(119) Brus, L. Growing Gold Nanoprisms with Light. *Nat. Mater.* **2016**, *15*, 824.
(120) Fu, Y.; Jia, G.; Pang, X.; Wang, R. N.; Wang, X.; Li, C. J.; Smemo, S.; Dai, Q.; Bailey, K. A.; Nobrega, M. A.; et al. Fto-Mediated Formation of N6-Hydroxymethyladenosine and N6-Formyladenosine in Mammalian Rna. *Nat. Commun.* **2013**, *4*, 1798.
(121) Pan, T. N6-Methyl-Adenosine Modification in Messenger and Long Non-Coding Rna. *Trends Biochem. Sci.* **2013**, *38*, 204−209.
(122) Zheng, G.; Dahl, J. A.; Niu, Y.; Fedorcsak, P.; Huang, C.-M.; Li, C. J.; Vågbø, C. B.; Shi, Y.; Wang, W.-L.; Song, S.-H.; et al. Alkbh5 Is a Mammalian Rna Demethylase That Impacts Rna Metabolism and Mouse Fertility. *Mol. Cell* **2013**, *49*, 18−29.
(123) Ye, F.; Zhang, L.; Jin, L.; Zheng, M.; Jiang, H.; Luo, C. Repair of Methyl Lesions in RNA by Oxidative Demethylation. *MedChemComm* **2014**, *5*, 1797−1803.
(124) Xie, L.-J.; Wang, R.-L.; Wang, D.; Liu, L.; Cheng, L. Visible-Light-Mediated Oxidative Demethylation of N6-Methyl Adenines. *Chem. Commun.* **2017**, *53*, 10734−10737.
(125) Shaik, F.; Peer, I.; Jain, P. K.; Amirav, L. Plasmon-Enhanced Multicarrier Photocatalysis. *Nano Lett.* **2018**, *18*, 4370−4376.
(126) Zhang, Y.; Aslan, K.; Previte, M. J. R.; Geddes, C. D. Plasmonic Engineering of Singlet Oxygen Generation. *Proc. Natl. Acad. Sci. U. S. A.* **2008**, *105*, 1798−1802.
(127) Planas, O.; Macia, N.; Agut, M.; Nonell, S.; Heyne, B. Distance-Dependent Plasmon-Enhanced Singlet Oxygen Production and Emission for Bacterial Inactivation. *J. Am. Chem. Soc.* **2016**, *138*, 2762−2768.
(128) Lv, J. L.; Wu, G. Q.; He, Y.; Zhang, L. J.; Yi, Y. H. Methylene Blue-Loaded Gold Nanobipyramids @SiO_2 Enhanced Singlet Oxygen Generation for Phototherapy of Cancer Cells. *Opt. Mater. Express* **2017**, *7*, 409−414.
(129) Tardivo, J. P.; Del Giglio, A.; de Oliveira, C. S.; Gabrielli, D. S.; Junqueira, H. C.; Tada, D. B.; Severino, D.; Turchiello, R. D. F.; Baptista, M. S. Methylene Blue in Photodynamic Therapy: From Basic Mechanisms to Clinical Applications. *Photodiagn. Photodyn. Ther.* **2005**, *2*, 175−191.
(130) Baciocchi, E.; Del Giacco, T.; Lapi, A. Oxygenation of Benzyldimethylamine by Singlet Oxygen. Products and Mechanism. *Org. Lett.* **2004**, *6*, 4791−4794.
(131) Baciocchi, E.; Del Giacco, T.; Lapi, A. Quenching of Singlet Oxygen by Tertiary Aliphatic Amines. Structural Effects on Rates and Products. *Helv. Chim. Acta* **2006**, *89*, 2273−2280.
(132) Baciocchi, E.; Del Giacco, T.; Lanzalunga, O.; Lapi, A. Singlet Oxygen Promoted Carbon-Heteroatom Bond Cleavage in Dibenzyl Sulfides and Tertiary Dibenzylamines. Structural Effects and the Role of Exciplexes. *J. Org. Chem.* **2007**, *72*, 9582−9589.
(133) Belvedere, A.; Bosca, F.; Cuquerella, M. C.; de Guidi, G.; Miranda, M. A. Photoinduced N-Demethylation of Rufloxacin and Its Methyl Ester Under Aerobic Conditions. *Photochem. Photobiol.* **2002**, *76*, 252−258.
(134) Gorman, A. A.; Gould, I. R.; Hamblett, I.; Standen, M. C. Reversible Exciplex Formation Between Singlet Oxygen, 1-Delta-G, and Vitamin-E - Solvent and Temperature Effects. *J. Am. Chem. Soc.* **1984**, *106*, 6956−6959.
(135) Gould, I. R.; Young, R. H.; Mueller, L. J.; Farid, S. Mechanisms of Exciplex Formation - Roles of Superexchange, Solvent Polarity, and Driving-Force for Electron-Transfer. *J. Am. Chem. Soc.* **1994**, *116*, 8176−8187.
(136) Phan, H. T.; Haes, A. J. Impacts of Ph and Intermolecular Interactions on Surface-Enhanced Raman Scattering Chemical Enhancements. *J. Phys. Chem. C* **2018**, *122*, 14846−14856.
(137) Habteyes, T. G. Direct near-Field Observation of Orientation-Dependent Optical Response of Gold Nanorods. *J. Phys. Chem. C* **2014**, *118*, 9119−9127.
(138) Habteyes, T. G.; Dhuey, S.; Kiesow, K. I.; Vold, A. Probe-Sample Optical Interaction: Size and Wavelength Dependence in Localized Plasmon near-Field Imaging. *Opt. Express* **2013**, *21*, 21607.
(139) Zrimsek, A. B.; Chiang, N. H.; Mattei, M.; Zaleski, S.; McAnally, M. O.; Chapman, C. T.; Henry, A. I.; Schatz, G. C.; Van Duyne, R. P. Single-Molecule Chemistry with Surface- and Tip-Enhanced Raman Spectroscopy. *Chem. Rev.* **2017**, *117*, 7583−7613.
(140) Lee, J. H.; Tallarida, N.; Chen, X.; Liu, P. C.; Jensen, L.; Apkarian, V. A. Tip-Enhanced Raman Spectromicroscopy of Co(Ii)-Tetraphenylporphyrin on Au(111): Toward the Chemists' Microscope. *ACS Nano* **2017**, *11*, 11466−11474.
(141) Harvey, C. E.; Weckhuysen, B. M. Surface- and Tip-Enhanced Raman Spectroscopy as Operando Probes for Monitoring and Understanding Heterogeneous Catalysis. *Catal. Lett.* **2015**, *145*, 40−57.
(142) Lee, J.; Tallarida, N.; Chen, X.; Jensen, L.; Apkarian, V. A. Microscopy with a Single-Molecule Scanning Electrometer. *Sci. Adv.* **2018**, *4*, eaat5472.
(143) Bockmann, H.; Gawinkowski, S.; Waluk, J.; Raschke, M. B.; Wolf, M.; Kumagai, T. Near-Field Enhanced Photochemistry of Single Molecules in a Scanning Tunneling Microscope Junction. *Nano Lett.* **2018**, *18*, 152−157.
(144) Hollerer, M.; Lüftner, D.; Hurdax, P.; Ules, T.; Soubatch, S.; Tautz, F. S.; Koller, G.; Puschnig, P.; Sterrer, M.; Ramsey, M. G. Charge Transfer and Orbital Level Alignment at Inorganic/Organic Interfaces: The Role of Dielectric Interlayers. *ACS Nano* **2017**, *11*, 6252−6260.
(145) Zhang, X.; Li, X. Q.; Reish, M. E.; Zhang, D.; Su, N. Q.; Gutierrez, Y.; Moreno, F.; Yang, W. T.; Everitt, H. O.; Liu, J. Plasmon-Enhanced Catalysis: Distinguishing Thermal and Nonthermal Effects. *Nano Lett.* **2018**, *18*, 1714−1723.

DOI: 10.1021/acs.jpcc.8b12054
J. Phys. Chem. C 2019, 123, 8469−8483